Juni Khyat
(UGC Care Group I Listed Journal)
ISSN: 2278-4632
Vol-12 Issue-07 No.03 July 2022

Evaluation of Operational Features Based on Multilane Turbo Roundabouts with an Entropy Method

Sudesna Baliarshinga [1], Anita Gochhayat [2], Abhijeet Satapathy [3], Bharat Sahoo [4], Biswa Ranjan Mohalik [5], Sweta Panda [6], NITYANANDA SAHOO[7]
[1, 2, 3, 4, 5, 6] Gandhi Institute for Education & Technology, Baniatangi, Khordha, Odisha
[7]NM Institute of Engineering & Technology,Bhubaneswar,Odisha
sudesnabaliarsingh@giet.edu.in, anitagochhayat@giet.edu.in, abhijeetsatapathy@giet.edu.in, bharatsahoo@giet.edu.in, biswa

Abstract: Conventional four-legged crossings are prone to congestion issues and inefficient under large traffic demand. Unusual crossroads with creative designs enable more effective traffic operations and, in certain situations, can improve the intersection's capacity. The upstream signalised crossover intersection (USC), continuous flow intersection (CFI), and parallel flow junction are examples of common atypical designs for four-legged intersections (PFI). These unusual designs are currently being used by an increasing number of communities to enhance the functionality of their crossings. As a result, we chose a typical crossroads in Xi'an for optimization and looked into the intersection's traffic statistics. The VISSIM programme was used to assess the traffic operations in relation to the USC, CFI, and PFI four options for a standard junction. The CRITIC (CRiteria Importance Through Intercriteria Correlation) method, a multi-criteria decision-making (MCDM) method that enables a more thorough and integrated evaluation of the four solutions by taking into account the comparative intensities and conflicting character among the indices, was then used to assess the suitability of each solution under various circumstances. According to the findings, the conventional intersection is only useful in situations with extremely low traffic volumes; in situations with moderate to high volumes of traffic, PFI performs better; in situations with high volumes of traffic, CFI performs better; and in situations with very low volumes of traffic, USC performs worse than CFI and PFI on average, though it occasionally improves more than the conventional solution.

Keywords: unconventional four-legged intersection; USC; CFI; PFI; VISSIM; MCDM; CRITIC method

1. Introduction

Intersections are essential nodes in the urban traffic network, where the capacity of the intersection largely determines the fluency of the entire urban road network. With the rapid growth of the urban population and the number of vehicles, urban intersections are increasingly becoming a bottleneck in urban road networks [1–3]. When the number of vehicles increases sharply, the traffic flow in different directions at each intersection also increases, leading not only to worse congestion in merging regions [4,5], but also to more serious problems involving the passage of left-turning traffic [6]. The problem of left turns at urban intersections has long been considered a challenge.

For general intersections, when left-turning traffic operates, there will be conflict points with the traffic in the straight direction, which not only causes congestion but also poses safety hazards [7,8]. To ensure the safe passage of left-turning traffic, separate left-turning phases need to be set for left-turning traffic; however, this can increase traffic delays [9,10]. For large intersections, in order to be able to reduce delays, left-turn waiting areas are

ISSN: 2278-4632
Vol-12 Issue-07 No.03 July 2022

usually provided, in order to improve the efficiency of left-turning traffic [11,12], but the signal timing at the intersection is still four-phase, which is a very limited improvement for intersections. Therefore, attempts have been made to maximize the potential of traditional typical intersections as much as possible, starting with optimizing the signal timing [13–15]. The traffic signal is an important factor affecting the operation of vehicles at intersections and setting the optimal scenario for traffic lights on intersections is very important and urgent. There exist diverse signal timing optimization models for intersections based on various algorithms and models [6,16,17]; for example, the signal timing of intersections has been optimized by adopting a meta-heuristic algorithm with difference operator [18]. Then, intersections showed considerable improvements, especially in capacity, delays, and emissions. In addition, traffic light phase control algorithms for different density roads are evaluated and improved [19]. The multi-intersection co-operative traffic signal control method, based on different algorithms [20,21], can co-ordinate and optimize the signal timing of multiple intersections, effectively reducing the delay time of each intersection in the road network and improving the capacity of the whole road network. Using the special left-turn signal control method [22], the left-turn lane can be turned into a controllable shared lane for both left-turning and straight traffic, which can improve the efficiency of the entire intersection. In addition, the use of signal transit priority for buses [23–25] is an effective way to improve urban traffic operations in cities, especially on roads with numerous buses. The optimization of signal timing at conventional intersections has been proven to provide great improvement for the capacity of intersections; however, with the dramatic growth of traffic, the capacity of traditional intersections has gradually failed to meet the vehicle travel demand.

In order to further improve the capacity of intersections, some novel measures have been proposed. In terms of lane usage, dynamic reversible lanes [26] can be provided between two adjacent intersections, in order to enhance their capacity. Similarly, dynamic exit lanes [27,28] designed specifically for left-turning vehicles can be used to accommodate left-turning vehicles in a single intersection. They are both designed similarly to tidal lanes, in order to increase lane usage while guaranteeing the capacity of intersections. In terms of traffic organization, the Same Entrance Full-Pass (SEFP) approach [29] allows vehicles from the same entrance to be released at the same time, thereby ensuring that all vehicles from the same entrance pass directly through the critical intersection without stopping, which is used to prevent the oversaturation of critical intersections during peak hours. In terms of computer applications, digital information and internet technologies can be used to create dynamic control systems that integrate roads, vehicles, and the environment [30–32] to achieve the dynamic management of vehicles, thereby improving the capacity and safety of intersections.

The design and study of unconventional intersections have attracted significant attention, which not only due to their unique shapes and structures, but more considerably for their variety and ability to optimize the operations of left-turn and straight traffic flow within the intersection by their own unique properties and advantages, largely improving the capacity and safety of the intersection meanwhile reducing emissions [33–35]. The advantages of this unconventional structural design are particularly evident in non traffic lighted intersections, such as unconventional roundabouts [36,37]. Unconventional intersections mainly include the conventional median U-turn design (MUT), the unconventional median U-turn design, super street median design (SSM), the Bowtie design, the Jughandle design, the quadrant roadway intersection design (QR), the split intersection, unconventional roundabouts (elliptical, turbo roundabouts, and so on), the double crossover intersection (DXI), the upstream signalized crossover intersection (USC), the continuous flow intersection (CFI), the parallel flow intersection (PFI), unconventional, and so on. Three of these unconventional designs—USC, CFI, and PFI—which are often used by designers, have similar characteristics. They are signal-controlled intersections and symmetrical in structure, can be used for the improvement of four-legged intersections and, most importantly, they are all based on the principle of changing the original traffic

ISSN: 2278-4632
Vol-12 Issue-07 No.03 July 2022

organization through four secondary intersections, such that the left-turning traffic and straight traffic can be carried out in one signal phase, reducing the signal timing of intersections from four phases to two phases in one cycle, in which the two-phase signal design can significantly enhance the intersection capacity [38]. Not only that, but their structure can be adjusted to allow for the modification of only one or two legs of the intersection that need to be improved [39,40].

An upstream signalized crossover intersection (USC) eliminates the conflict between left-turning and straight traffic at the main intersection, by changing the straight and left-turning traffic from right-hand traffic to left-hand traffic through four secondary intersections; ultimately, it can ensure that the straight and left-turning vehicles at the main intersection can operate simultaneously, through controlling the main intersection and four secondary intersections by two-phase signals. This unconventional design can significantly reduce delays, compared to conventional intersections. Furthermore, when traffic volumes are highly unbalanced, USC has also shown great potential in most cases [41,42].

A continuous flow intersection (CFI), which has been recognized as a desirable unconventional design, separates the left-turning traffic in each direction to the outermost side (through four secondary intersections) and ensures that there is no conflict between straight and left-turning vehicles at the main intersection and that the two flows can operate simultaneously. The primary and secondary intersections of CFI are also controlled by two-phase signals. In recent years, CFI has been studied in various aspects, including: the supplementation and study of CFI operational evaluation parameters [43], CFI signal timing optimization [44–46], pedestrian performance within CFI [47], and even the use of simplified and economical CFI [48,49] to optimize the properties of intersections when conditions are constrained. In general, the operational performance of CFI is evident and its delay can be significantly reduced [50–52], while the capacity can be significantly increased [53], compared to conventional intersections.

A parallel flow intersection (PFI) is a cost-saving design. Its structure is similar to that of the CFI, where the difference is that the left-turning traffic passes through the main intersection into the exit lane in a CFI while, in a PFI, the left-turning traffic passes through the main intersection into the inlet lane between the straight and right-turning lanes [54]. The major intersection and secondary intersections of a PFI also use two-phase control, but the traffic organization is different from CFI, where the left-turning traffic in the CFI's major intersection runs together with the straight-through traffic in the same direction, while the left-turning traffic at PFI's major intersection runs together with the straight-through traffic on the intersecting roads. As a design of the same level as CFI, PFI provides considerable improvements over conventional intersections, in terms of capacity, safety, and delays [55].

The three types of intersections previously mentioned—USC, CFI, and PFI—have certain similarities, such that the comparative study of these three intersections is critical and necessary, affecting exactly how decision-makers and designers make use of them in the future. Currently available studies have shown that CFI has the lowest travel time among the seven common unconventional intersection designs [34]. Between CFI and USC, both have better capacity improvements, compared to the conventional solution, at moderate and high traffic volumes, but CFI performs better than USC [56]. Between CFI and PFI, the delays are similar when the traffic volume is low, while the delays are lower for CFI when the traffic volume is higher [57]. In addition, the different geometries of the three types of intersections, the traffic volume, and the signal timing affect their capacity and delay improvements [56,58].

The current study is adequate for these three kinds of intersections individually, but there are some shortcomings in how to compare and evaluate these unconventional intersections with a more integrated approach. In terms of indices, the evaluation indices selected in the current study are mainly related to delays, followed by queue length and capacity, which belong to traffic indices. Environmental indices, such as carbon emissions and fuel consumption, are not considered. With the concept of sustainable development sinking deep into the hearts of the people, it is increasingly crucial to consider

ISSN: 2278-4632
Vol-12 Issue-07 No.03 July 2022

transportation and environmental issues in an integrated manner [59]. In the typically used methods, only a simple comparison of each index is made through simulation, without linking the indices to each other for comprehensive consideration. In terms of comparison scope, only a small portion of the traffic volume was selected for comparison, and the coverage was not comprehensive enough. Such simple comparisons cannot provide complete guidance to decision-makers and designers in the selection of solutions.

Multi-criteria decision-making (MCDM) is a scientific and effective method that analyzes the impact factors of indices by calculating the weights of different indices and then scoring them in a comprehensive way. MCDM is a branch of operations research that studies the analysis of finding optimal results in complex situations [60]. In the context of the global implementation of a low-carbon economy, MCDM has become increasingly popular for the assessment of environmental protection and energy conservation [60,61]. In MCDM, it is often necessary to judge the importance of indices by calculating the weights of evaluation indices, where the commonly used methods for objectively calculating the weights of indices include the entropy evaluation method, the CRITIC method, and so on. The entropy method, which determines the magnitude of the weights of indices by their confusion, is simple to calculate and has been applied for the comprehensive assessment of intersections [62,63]. However, the entropy method cannot consider the connection between each index and has certain limitations. The CRITIC method is based on the quantification of the two basic concepts of MCDM, and calculates the weights of indices through the comparative intensity and the conflicting nature of indices, taking into account both the trends of individual indices and the correlations between them [64]. It has been widely used in manufacturing [65,66], construction applications [67,68], internet cloud services [69], medical pharmacy [70], electrical grid systems [71], and the sustainable optimization of energy and environment [72–74], among other interdisciplinary subjects.

The main objective of this paper is to use the CRITIC method to carry out a comprehensive evaluation of USC, CFI, and PFI under different combinations of traffic volumes, selecting maximum queue length, number of vehicles, delays, number of stops, and travel time as traffic indices, and CO emissions and fuel consumption as environmental indices. Ultimately, the optimal solution for different situations is selected through the multi-criteria decision-making method. The rest of the paper is organized as follows: Section 2 illustrates the actual case analysis and data collection. Section 3 presents the modeling of intersections for four improvement solutions, including USC, CFI, and PFI, in VISSIM and the analysis of simulation results. Section 4 presents the sensitivity analysis of each solution under different traffic scenarios. Section 5 discusses the process of calculating the weights of indices by the CRITIC method, and the optimal solution is derived. Our final conclusions are drawn in Section 6, see Figure 1.

ISSN: 2278-4632
Vol-12 Issue-07 No.03 July 2022

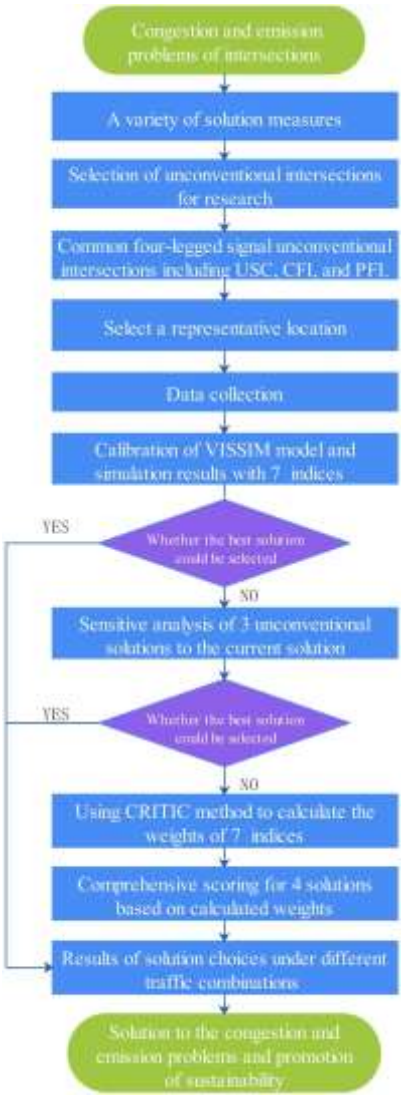

Figure 1. Flowchart of selecting signal unconventional intersections with the CRITIC method.

2. Problem Statement and Data Collection

2.1. Problem Statement

Xi'an is a city with a long history and a fast-growing transportation industry [75]. As of the end of 2019, the population of Xi'an exceeded 10.2 million. Furthermore, as of 25 October 2020, the number of motor vehicles in the city had reached 3.7 million, an increase by 681,000 from March 2019, which continues to grow at a high rate [76].

With the growing number of vehicles within the city and the size limitations of the city roads, its arterial roads and intersections have become overwhelmed during the morning and evening peaks. For intersections, the traditional intersection capacity can no longer meet the increasing vehicle demand. Therefore, in order to maximize the capacity of intersections and road service level, it would be very effective to improve the traffic organization of intersections, through the use of unconventional intersections in the design of new intersections, as well as in the reconstruction of existing intersections. There exist various types of unconventional intersections, the most common of which are USC, CFI, and PFI, all of which have common characteristics: They ensure the effective passage of left-turning vehicles through special traffic organization, which can effectively reduce the number of conflict points of vehicles in the range of intersections, especially eliminating the conflict points of left-turning and straight traffic, thus ensuring that left-turning vehicles can run simultaneously with straight and right-turning vehicles. Some cities in China have

ISSN: 2278-4632
Vol-12 Issue-07 No.03 July 2022

started to improve the performance of intersections by adopting unconventional designs. For some cities, such as Xi'an, the urban structure is distributed as a regular rectangle with well-defined directions, and most of the large intersections are symmetrical in structure and the roads are orthogonal to each other. In such a case, it is more convenient and suitable to adopt these unconventional designs for intersection improvements.

However, there are many existing intersections and many new intersections need to be built as the city expands. When reconstruction or new construction is carried out, the question of which type of unconventional intersection is better becomes of great significance.

Based on the CRITIC method, we adopted the multi-criteria decision-making method and took Xi'an XiaoZhai intersection as an example, focusing on a comprehensive comparison of four types of intersections—conventional, USC, CFI, and PFI—and proposed the respective scope of application for the three improvement solutions (i.e., USC, CFI, and PFI).

2.2. *Data Collection*

Actual collected traffic data are needed for model calibration and micro-simulation in VISSIM. In this paper, we took XiaoZhai intersection as an example, due to its high traffic volume, frequent congestion, and high delay, as shown in Figure 2. The congestion index of Xi'an can be obtained, according to the statistics of the AutoNaviTraffic in ChinaCompany [77]. According to the congestion index, the morning peak of Xi'an occurs between 7:00 a.m. and 9:00 a.m., while the evening peak occurs between 5:00 p.m. and 7:00 p.m. The congestion index of Xi'an, for the whole day of 23 October, 2020, is shown in Figure 3. Therefore, the corresponding peak hours were selected, in order to collect traffic data for the morning, midday, and evening peaks at the XiaoZhai intersection. It was also ensured that the weather conditions and road conditions were favorable and free from construction zones and traffic accidents.

Figure 2. The investigated intersection location scheme. The investigated intersection is a four-legged intersection located in the center of Xi'an XiaoZhai. The arterial street is a North–South six-lane road, while the secondary street is a West–East six-lane road.

The instruments used to collect data were mainly cameras and radars, where the cameras were used for traffic volume counting and the radars used to collect vehicle speeds and trajectories.

The data to be collected included the current signal timing; the traffic counts; the proportion of left-turning, straight-ahead, and right-turning vehicles at each inlet; the

ISSN: 2278-4632
Vol-12 Issue-07 No.03 July 2022

proportion of different vehicle types; and the operating speeds of vehicles within the intersection.

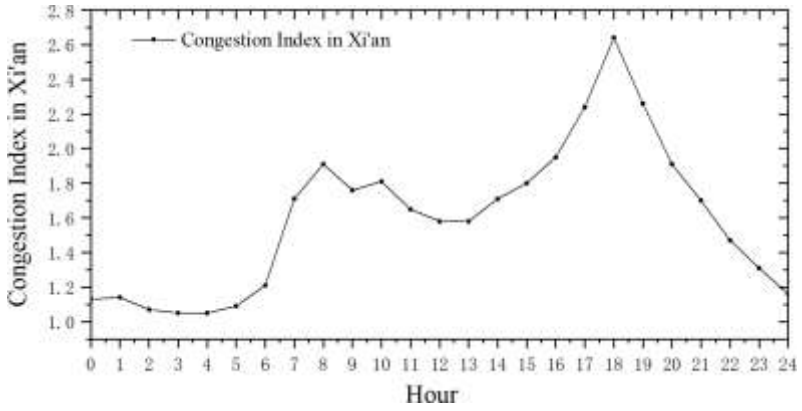

Figure 3. The congestion index in Xi'an on 23 October 2020. The real-time congestion index can be obtained from the Autonavi Company Webpage at https://report.amap.com/detail.do?city=610100 (accessed on 23 October 2020).

Figure 4a shows a map of the location of the monitoring stations. To represent the intersection more clearly, a schematic diagram of the current intersection is given by Figure 4b. Figure 5 shows the arrangement of equipment of the data collection for the current intersection. Standing on the pedestrian bridge, the surveyor put the camera and radar at four directions of the intersection respectively for recording at 7:00 to 8:00 a.m., 12:00 to 1:00 p.m., and 7:00 to 8:00 p.m. on 23 October 2020.

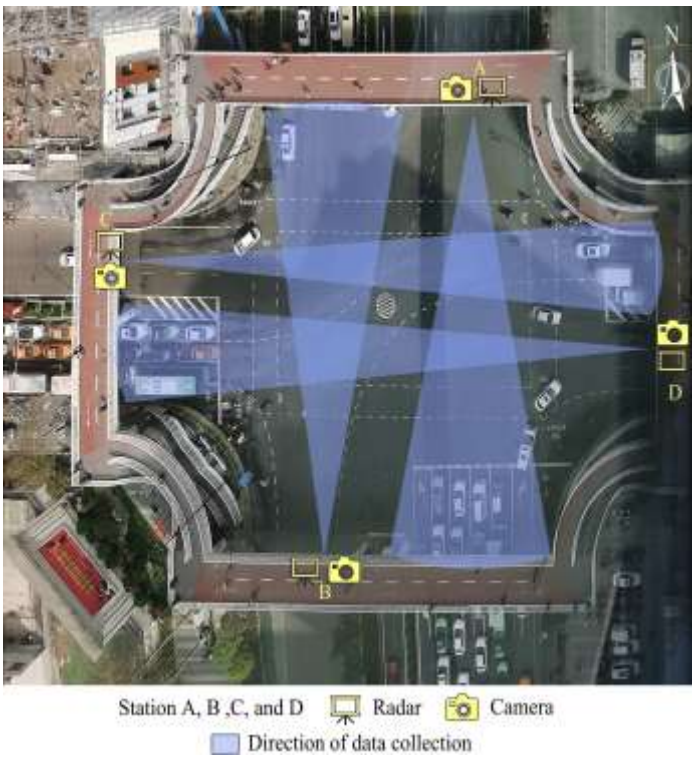

(a) Map of the location of the monitoring stations.

Figure 4. *Cont.*

ISSN: 2278-4632
Vol-12 Issue-07 No.03 July 2022

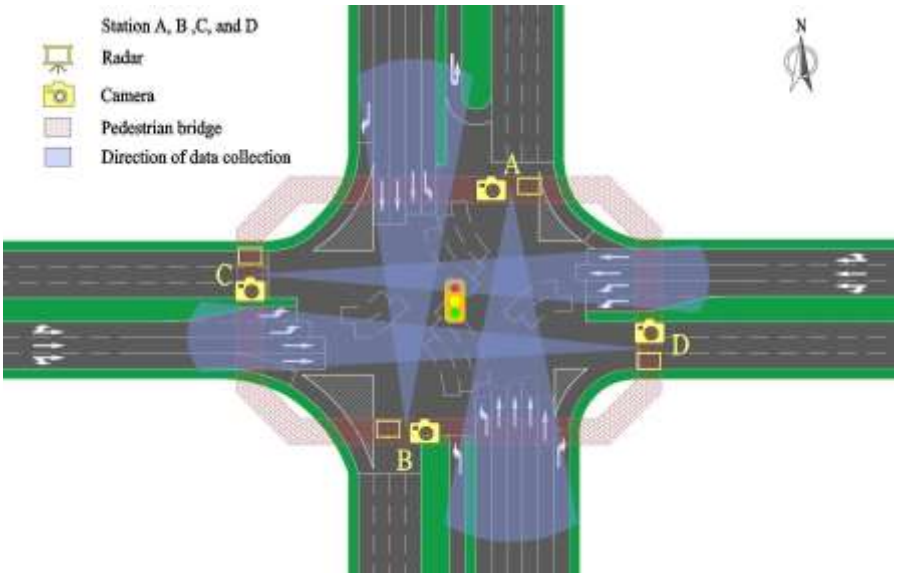

(b) Schematic diagram of the monitoring stations.

Figure 4. The location of the monitoring stations at the current intersection. Coordinates of the current intersection: 108.953216, 34.22907.

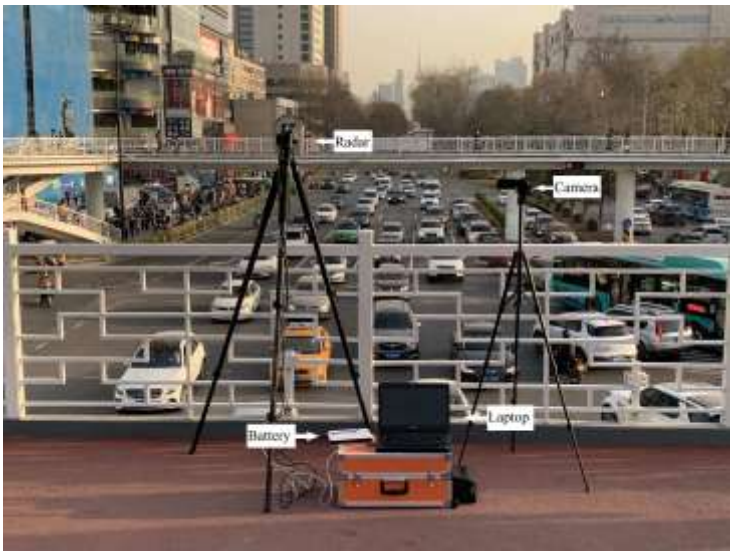

Figure 5. The arrangement of equipment of data collection for each monitoring station.

After data and statistics collection, traffic volume measured at Xiaozhai intersection was 7131 veh/h in the morning peak hour, 6142 veh/h in the midday peak hour, and 6648 veh/h in the evening peak hour. As the traffic volume was the highest in the morning peak hour, the traffic volume in the morning peak hour was chosen as a representative. Table 1 shows the collected data of the morning peak period over 1 h.

ISSN: 2278-4632
Vol-12 Issue-07 No.03 July 2022

Table 1. Collected data during one peak hour (7:30 a.m. to 8:30 a.m.) on 23 October 2020.

Direction	Turn	Flow	Car	Bus	Truck	Average Speed (km/h)	Min. Speed (km/h)	Max. Speed (km/h)
North to South	S	1	1219	154	0	21.58	0	65.43
	L	2	278	41	0	17.15	0	53.28
	R	3	293	23	4	15.86	0	56.94
	T	4	143	4	2	13.29	0	45.27
South to Nouth	S	5	1897	130	4	25.83	0	69.84
	L	6	328	18	0	17.91	0	52.63
	R	7	317	40	4	16.99	0	57.68
East to West	S	8	694	41	0	19.21	0	64.81
	L	9	120	34	0	17.85	0	39.60
	R	10	233	11	0	16.99	0	52.51
West to East	S	11	548	68	11	19.64	0	63.24
	L	12	210	19	0	17.96	0	48.60
	R	13	221	23	8	17.04	0	54.62

The minimum speed of 0 km/h means that vehicles had stopped and then moved. S, L, R, and T indicate vehicles going straight, turning left, turning right, and turning around, respectively.

The data collected revealed the following characteristics:

1. The two intersecting roads at the intersection had obvious primary and secondary characteristics, where the north–south direction was the main road, the east–west direction was the secondary road, and the traffic volume in the north–south direction was higher than the traffic volume in the east–west direction.
2. The total traffic volumes at the intersection were nearly the same for northbound and southbound, and nearly the same for eastbound and westbound.
3. The proportion of left-turning vehicles at the intersection was nearly the same for northbound and southbound (14.78% and 12.63%, respectively), and the proportion of left-turning traffic was relatively close for eastbound and westbound (13.58% and 20.69%, respectively).
4. The proportion of vehicles making a U-turn was not large.
5. The maximum speed of vehicles approached 70 km/h, while the average speed was only about 20 km/h, meaning that most of the vehicles were not moving fast.
6. The signal cycle was 175 s, and the split times were the same for southbound and northbound; the westbound straight and left-turn phases started and ended at the same time, while the eastbound straight phase started first, the left-turn phase started later and, finally, the straight and left-turn phases ended at the same time. It is worth noting that there was a period of time when the green light was on simultaneously for westbound left-turning vehicles and eastbound straight-through vehicles, which indicates a conflict point between left-turning and straight-through vehicles.
7. There was a waiting area at the intersection. The northbound and southbound left-turn waiting area contained three lanes, while the eastbound and westbound left-turn waiting area contained two lanes.
8. In 2020, the proportion of new-energy vehicle was 2.83% in Xi'an [78]. Therefore, the vehicles studied in this paper were traditional vehicles only.

3. Establishment and Simulation of the Model in VISSIM

3.1. Modeling of Each Solution

3.1.1. Geometric Design

Based on the traffic volume, the proportion of left-turning vehicles, the measured average speed, the maximum and minimum speeds, and previous studies on the geometry of USC, CFI, and PFI [42,56,58,79,80], the geometry of the proposed model is shown in Figure 6.

ISSN: 2278-4632
Vol-12 Issue-07 No.03 July 2022

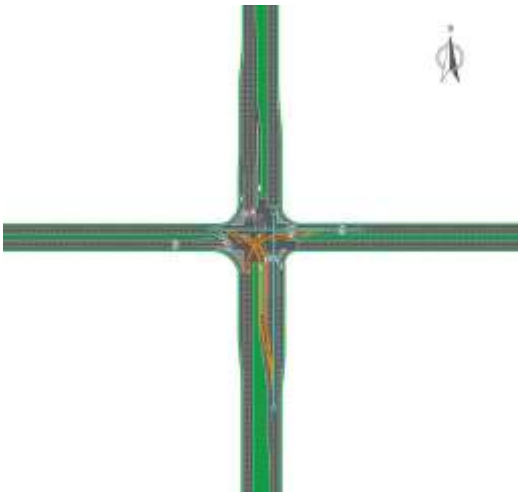

(a) Conventional Solution.

(b) USC.

(c) CFI.

Figure 6. *Cont.*

ISSN: 2278-4632
Vol-12 Issue-07 No.03 July 2022

(d) PFI.

Figure 6. Geometries of four solutions, including: (**a**) Conventional solution; (**b**) USC; (**c**) CFI; and (**d**) PFI. Blue lines indicate going straight traffic and orange lines suggest turning left.

Figure 6a shows the geometry of the current intersection. Because of the right-hand traffic in Xi'an, the geometric shapes of USC, CFI, and PFI in this paper adopt the right-hand traffic design.

Figure 6b illustrates the geometry of the USC. This design changing the straight and left-turning traffic from right-hand traffic to left-hand traffic through four secondary intersections; ultimately, it can ensure that the straight and left-turning vehicles at the main intersection can operate simultaneously.

Figure 6c presents the geometry of the CFI. CFI separates the left-turning traffic in each direction to the outermost side (through four secondary intersections) and ensures that there is no conflict between straight and left-turning vehicles at the main intersection and that the two flows can operate simultaneously.

Figure 6d shows the geometry of the PFI. Its structure is similar to that of the CFI, where the difference is that the left-turning traffic passes through the main intersection into the exit lane in a CFI while, in a PFI, the left-turning traffic passes through the main intersection into the inlet lane between the straight and right-turning lanes. The traffic organization of PFI is different from CFI, where the left-turning traffic in the CFI's major intersection runs together with the straight-through traffic in the same direction, while the left-turning traffic at PFI's major intersection runs together with the straight-through traffic on the intersecting roads.

From the geometric shapes of USC, CFI, and PFI, it can be said that the primary and secondary intersections of these three unconventional designs are controlled by two-phase signals, which greatly facilitate the operation of the vehicles.

3.1.2. Signal Phasing and Timing

The Synchro software has been used by many traffic engineers, in order to determine signal cycles and to optimize and co-ordinate signal timing. Synchro can calculate the signal timing of unconventional intersections, such as USC and CFI, and has shown good performance in optimizing the signal timing of these unconventional intersections [42,58]. As Synchro's processing is iterative, it calculates the delays, queuing, and vehicle stops of the network while adjusting the signal timing. It then assigns a score to each iteration, based on these effectiveness metrics, to achieve optimal network signal timing [42].

In this paper, we use the synchro7 software to determine the signal timing of four types of intersections, including conventional intersection (present solution), USC, CFI, and PFI, under different traffic scenarios.

ISSN: 2278-4632
Vol-12 Issue-07 No.03 July 2022

3.2. Calibration of Vissim Model

In this paper, VISSIM is used for microscopic simulation, in order to analyze the regularity of the simulation results, which is crucial to ensure the accuracy of the simulation model, such that VISSIM provides reasonable capacity estimates for all movements [81]. The model calibration in this stage followed the normal calibration procedures proposed in previous studies [82–84]. Several calibrated parameters are available in the VISSIM simulation model: the gap-accepting model, car-following model, and lane-changing model. However, capacity is the most commonly used metric, as it is very sensitive to route selection behavior, so it is mainly used for route selection in road network calibration. Calibration with capacity indicators consists of two main steps:

1. First, the capacity of each flow needs to be determined, which can be calculated by (1):

$$C = \frac{3600}{\overline{h_t}}, \tag{1}$$

where C denotes the ideal capacity (veh/h) and $\overline{h_t}$ denotes the average minimum headway(s).

2. The MAPE index represents the mean absolute percentage error, which is used to reflect the error between the actual collected and simulated capacity of each flow. The MAPE can be calculated according to (2):

$$MAPE = \frac{\sum_{a=1}^{n} C_v^a - \sum_{a=1}^{n} C_f^a}{\sum_{a=1}^{n} C_f^a}, \tag{2}$$

where a denotes the traffic flow, n denotes a total of 13 different traffic flows, C_v^a is the simulated capacity of VISSIM (veh/h), and C_f^a denotes the collected capacity (veh/h). Table 2 shows the calculated MAPE results for each traffic flow.

Table 2. VISSIM simulation calibration results with collected data.

Direction	Turn	Flow	Investigated Capacity (veh/h)	Simulated Capacity (veh/h)	MAPE for Each Flow (%)	MAPE (%)
Nouth to South	S	1	1373	1332	−3.0%	−3.2%
	L	2	319	247	−22.6%	
	R	3	319	325	2.1%	
	T	4	146	128	−12.3%	
South to Nouth	S	5	2030	1963	−3.3%	
	L	6	346	306	−11.5%	
	R	7	360	375	4.1%	
East to West	S	8	735	690	−6.1%	
	L	9	154	138	−10.2%	
	R	10	244	247	1.2%	
East to West	S	11	626	641	2.4%	
	L	12	229	256	12.1%	
	R	13	251	256	2.1%	

From the calculation results, it can be seen that the total error between the simulation model and the reality was −3.2%, indicating that the established VISSIM model error was within the acceptable range [85,86], and its accuracy was sufficient.

ISSN: 2278-4632
Vol-12 Issue-07 No.03 July 2022

3.3. VISSIM Calculation of Operational Measures

3.3.1. Selection of Evaluation Indices

The most common traffic indices used in VISSIM to evaluate intersection performance are delay, travel time, and number of stops [87,88]. In this paper, in order to evaluate the performance of several intersections more comprehensively, two indices—maximum queue length and the number of vehicles [87]—were additionally selected. Furthermore, in recent years, many cities have faced not only serious traffic congestion problems but also serious environmental problems, such as air pollution [89]. Vehicle emissions have a great impact on air pollution. In order to relieve traffic congestion and reduce air pollution from vehicle emissions, a number of cities have imposed vehicle traffic restrictions [90]. Based on environmental considerations, it is necessary to select environmental indices as part of the criteria for evaluating the performance of intersections. Therefore, CO emissions and fuel consumption [87] were selected as environmental indices in this paper.

3.3.2. Simulation Results

The actual collected traffic data were input into each of the four solution models for simulation. Table 3 shows the results of the seven indices for the four solutions. It is clear that the conventional solution performed the worst overall, but had the lowest number of stops. For the USC, the overall degree of optimization was not significant, only the degree of optimization in terms of travel time and delays was greater. On the other hand, CFI and PFI were two very well optimized solutions. There was a slight discrepancy between the two solutions, in terms of the number of vehicles, delays, maximum queue length, and fuel consumption, with CFI slightly outperforming PFI. CFI was superior to PFI, in terms of CO emissions and number of stops; however, for the travel time index, the PFI is better than the CFI.

Table 3. Simulation results of four solutions.

	Conventional	USC	CFI	PFI
Maximum Queue Length (m)	197.82	175.53	94.60	101.07
Number of Vehicles	959	955	982	976
Delay (s)	53.93	36.33	28.33	31.44
Number of Stops (times)	0.916	1.417	1.015	1.244
CO Emission (grams)	2176.53	2169.06	1852.53	2031.69
Fuel Consumption (gallon)	31.137	31.031	26.502	29.065
Travel Time (s)	1060.54	617.02	756.42	550.25

In order to achieve a visual effect, the results are plotted into a radar map. Except for the number of vehicles, the smaller the indices, the better. As Figure 7 shows, the axis of the number of vehicles is set opposite to the axes of other indices. Therefore, the area in the radar map reflects the performance of each solution, with larger area indicating worse performance.

In summary, the degree of USC improvement was not very significant, while CFI and PFI performed well, but each had its own advantages. Therefore, it was not possible to generalize which was better and which was worse for the three improvement solutions, especially CFI and PFI. A more comprehensive and integrated consideration is necessary.

ISSN: 2278-4632
Vol-12 Issue-07 No.03 July 2022

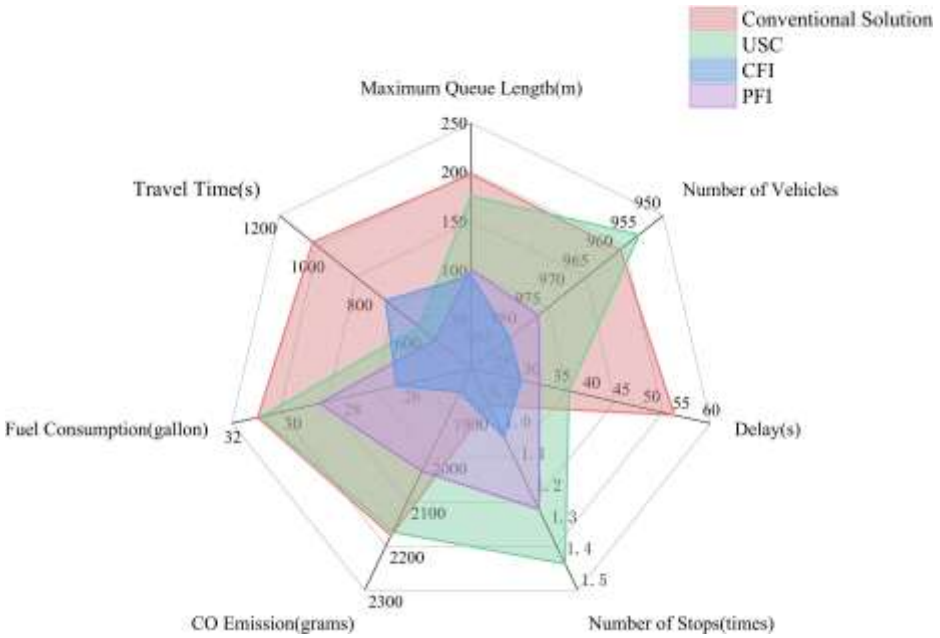

Figure 7. Performance of solutions 1, 2, 3, and 4. The larger area indicates the worse performance.

3.4. Safety Evaluation

A safety evaluation should be included for a complete simulation evaluation. A commonly used tool, the Surrogate Safety Assessment Model (SSAM), is a simulation and analysis project used by the Federal Highway Administration (FHWA) to predict road safety before an accident occurs. SSAM is a software application that not only automatically identifies, classifies, and evaluates traffic conflicts in the vehicle trajectory data output from microscopic traffic simulation models, but also has built-in statistical analysis of conflict frequency and severity, which can help analysts to design safe traffic facilities [91–93].

The collected morning peak traffic volumes were input into the four solutions, and a safety analysis was performed separately for each solution. Table 4 shows the results of the safety evaluation for the four solutions. For the crossing index, USC and PFI performed better, being 80.0% less than the conventional solution, while that of CFI was 50.0% less than the conventional solution. For rear-ending, the USC, PFI, and conventional solutions performed similarly, with only the CFI performing better (27.2% less than the conventional solution). For the number of vehicle lane changes, PFI performed the best, 56.3% less than the conventional solution, while those of USC and CFI were 35.4% and 41.7% less than the conventional solution, respectively. In general, the conventional solution had higher safety risks, USC had better improvement for conflict crashes, CFI had better improvement for rear-end crashes, and PFI had better improvement for conflict crashes and lane change behavior of the vehicles.

Table 4. Safety analysis of four simulations by SSAM.

Number	Item	Crossing	Rear End	Lane Change	Total
1	Conventional	20	206	48	274
2	USC	4	213	28	245
3	CFI	10	150	31	191
4	PFI	4	207	21	231

4. Sensitivity Analysis of Operational Performance

The simulation results in the previous section showed that both CFI and PFI are well-optimized for intersections at the currently collected traffic volumes, but both had advantages and disadvantages, in terms of different indices. However, the simulation only covered the current traffic volume and did not reflect the circumstances under other traffic

ISSN: 2278-4632
Vol-12 Issue-07 No.03 July 2022

volumes, which restricts the evaluation of the simulation effect for the unconventional intersection improvement solutions. Therefore, this section discusses the degree of optimization of the intersections for different traffic combinations, respectively, for the different solutions.

As mentioned in Section 2, the northbound and southbound traffic volumes at XiaoZhai intersection were nearly the same, and the eastbound and westbound traffic volumes were also close to each other. Therefore, in the sensitivity analysis, to reduce the workload, the traffic volumes in the two directions of northbound and southbound are kept the same (similarly for eastbound and westbound), while the proportion of traffic flow in each direction and the proportion of vehicle types are kept the same as the current. There were three lanes in the north–south direction at the intersection. The maximum service traffic volume of the three lanes was 3430 veh/h [94]. According to the actual traffic volume data collected, the southbound and northbound traffic volumes were 2261 veh/h and 2254 veh/h in the morning peak hour, 2084 veh/h and 2512 veh/h in the midday peak hour, and 2156 veh/h and 2736 veh/h in the evening peak hour, respectively. Therefore, in the sensitivity analysis, the range of traffic volume was chosen as 0.2–1.0 V/C, where the range was divided into nine equal parts at 0.1 V/C intervals (i.e., 686 veh/h to 3430 veh/h). There were also three lanes in the east–west direction at the intersection. However, according to the actual traffic data collected, the westbound and eastbound traffic counts were 1128 veh/h and 1006 veh/h in the morning peak hour, 741 veh/h and 825 veh/h in the midday peak hour, and 1133 veh/h and 1106 veh/h in the evening peak hour, all of which were far below the large service traffic volume limit of 3430 veh/h. Hence, for the east–west direction, the traffic volume selection range was 0.2–0.6 V/C in the sensitivity analysis, which was divided into five equal parts at 0.1 V/C intervals (i.e., 686 veh/h to 2058 veh/h). In this way, a total of 45 traffic volume combinations were available, and the actual collected traffic volumes were included in the selected range of combinations. The traffic combinations for the sensitivity analysis are specified in Table 5. The signal timing for each solution with different traffic combinations was obtained using the synchro7 software.

Table 5. VISSIM volume in sensitivity analysis.

Item	Value
N–S volume	686/1029/1372/1715/2058/2401/2744/3087/3430
E–W volume	686/1029/1372/1715/2058

In this paper, k denotes the kth group of traffic combinations, which takes values from 1 to 45. For example, k = 1 denotes 686 veh/h (E–W direction volume) × 686 veh/h(N–S direction volume), k = 2 denotes 686 veh/h (E–W direction volume) × 1029 veh/h (N–S direction volume) and so on, up to k = 45, which denotes 2058 veh/h (E–W direction volume) × 3430 veh/h (N–S direction volume).

In the sensitivity analysis, seven indices—delay, travel time, number of stops, number of vehicles, CO emissions, fuel consumption, and maximum queue length—were used for the evaluation of intersection performance. Figures 8–10 indicate the degree of improvement of USC, CFI, and PFI, relative to the conventional type of intersection (i.e., present solution) in the seven indices, respectively.

ISSN: 2278-4632
Vol-12 Issue-07 No.03 July 2022

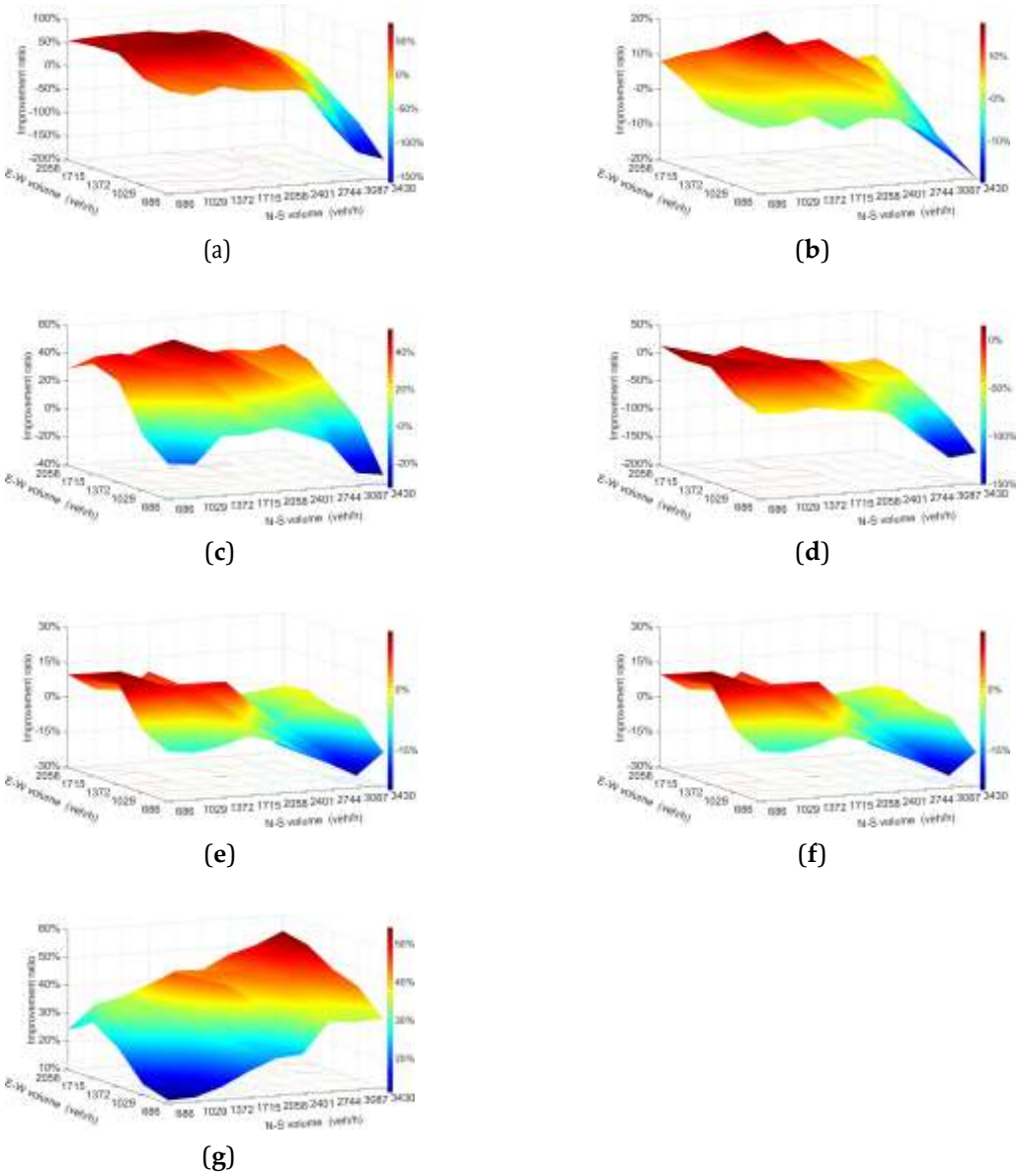

Figure 8. Improvement ratio of USC, compared with conventional solution: (**a**) maximum queue length; (**b**) number of vehicles; (**c**) delay; (**d**) number of stops; (**e**) CO emissions; (**f**) fuel consumption; and (**g**) travel time.

Figure 8a illustrates the degree of improvement in maximum queue length at USC, compared to the conventional solution, for the 45 traffic volume groups. When the traffic volume in the north–south direction was in the range of less than 2058 veh/h, the improvement of USC was better, where the maximum improvement reached 75.9%. When the east–west traffic volume was low and the north–south traffic volume was high, the maximum queue length of USC increased instead, with the lowest improvement of −15.9%, which was worse than the conventional solution.

Figure 8b reflects the comparison of the number of vehicles. Compared with the traditional solution, the overall improvement of USC for the number of vehicles was not high. When the traffic volume was large in the east–west direction and medium in the north–south direction, the improvement of USC was better, with the maximum reaching 17.7%; when the traffic volume was low in the east–west direction and high in the

ISSN: 2278-4632
Vol-12 Issue-07 No.03 July 2022

north–south direction, the USC solution was worse than the traditional solution, with the maximum being 19.9% worse than the traditional solution.

Figure 8c represents the results of the comparison between the USC and the conventional solution, in terms of delays. The delays of USC were lower than that of the conventional solution, in most cases. When the vehicles in the east–west direction gradually became larger, the better the improvement of USC, with the maximum improvement reaching 52.3%; however, when the traffic volume was small, the delays of USC were higher than the conventional solution, especially when the traffic volume in the east–west direction was small and the traffic volume in the north–south direction was large. In this case, the performance of USC was not as good as the conventional solution, and the delays were up to 33.8% higher than the conventional solution.

Figure 8d indicates the comparison of the number of stops for the two solutions. It is obvious that USC did not perform as well as the conventional solution, in most cases. Only when the traffic volume in the east–west direction was high and the traffic volume in the north–south direction was low did the number of stops of USC become less than that of the conventional solution, with a maximum improvement of only 14.7%. As the traffic volume in the east–west direction decreased and the traffic volume in the north–south direction increased, the number of stops of USC increased, compared with the conventional solution, with a maximum of 150.7% more than that of the conventional solution.

Figure 8e,f show the comparison of CO emissions and fuel consumption, respectively, between the two solutions. Due to the strong correlation between the two indices of CO emissions and fuel consumption, the trends of the two indices were essentially the same. When the traffic volume was high in the east–west direction and low in the north–south direction, the CO emissions and fuel consumption of USC were less than those of the conventional solution, with a maximum improvement of 14.2%. As the traffic volume increased in the north–south direction, the CO emissions and fuel consumption of USC gradually became higher than those of the conventional solution, with a maximum deterioration of 24.9%, compared to the conventional solution.

Figure 8g reflects the extent of USC's improvement in travel time. It is clear from the graph that USC completely outperformed the conventional solution and, as the east–west and north–south traffic volumes increased from small to large, the improvement also increased, from 11.1% to 54.1%.

Figure 9a shows that, for the maximum queue length, the minimum improvement of CFI was 19.1% and the maximum was 81.8% and, so, it is clear that CFI led to a considerable improvement in all cases, compared to the conventional solution. The degree of improvement had a certain regularity with the change of traffic volume in the east–west direction, as the degree of improvement increased with the rise of traffic volume in the east–west direction.

Figure 9b shows that the improvement of CFI, in terms of the number of vehicles, was better in the vast majority of cases, especially when the traffic volume was high in the east–west and north–south directions, where the improvement reached the maximum of 19.2%; however, when the traffic volume was low in the east–west direction, the improvement was ~~3.~~8%, thus being not as good as the conventional solution.

Figure 9c indicates that CFI had a satisfactory degree of improvement for delays. As the traffic volume in the east–west and north–south directions gradually increased, the improvement of CFI for delays also gradually increased. When the traffic volume was small, the improvement was ~~1~~5.5%, indicating that it was not as good as the conventional solution, in this case. However, in the vast majority of cases, it was better than the conventional solution, with a maximum improvement of 58.2%.

Figure 9d shows the comparison of the number of stops between the two solutions. Overall, CFI had more stops than the conventional intersection. The improvement in CFI was greater, up to 28.8%, only when the east–west traffic volume was high and the north–south traffic volume was low. However, as the traffic volume in the east–west direction

ISSN: 2278-4632
Vol-12 Issue-07 No.03 July 2022

decreased, the number of stops at CFI was gradually greater than that of the conventional intersection, becoming worse than the conventional solution by 52.1% at maximum.

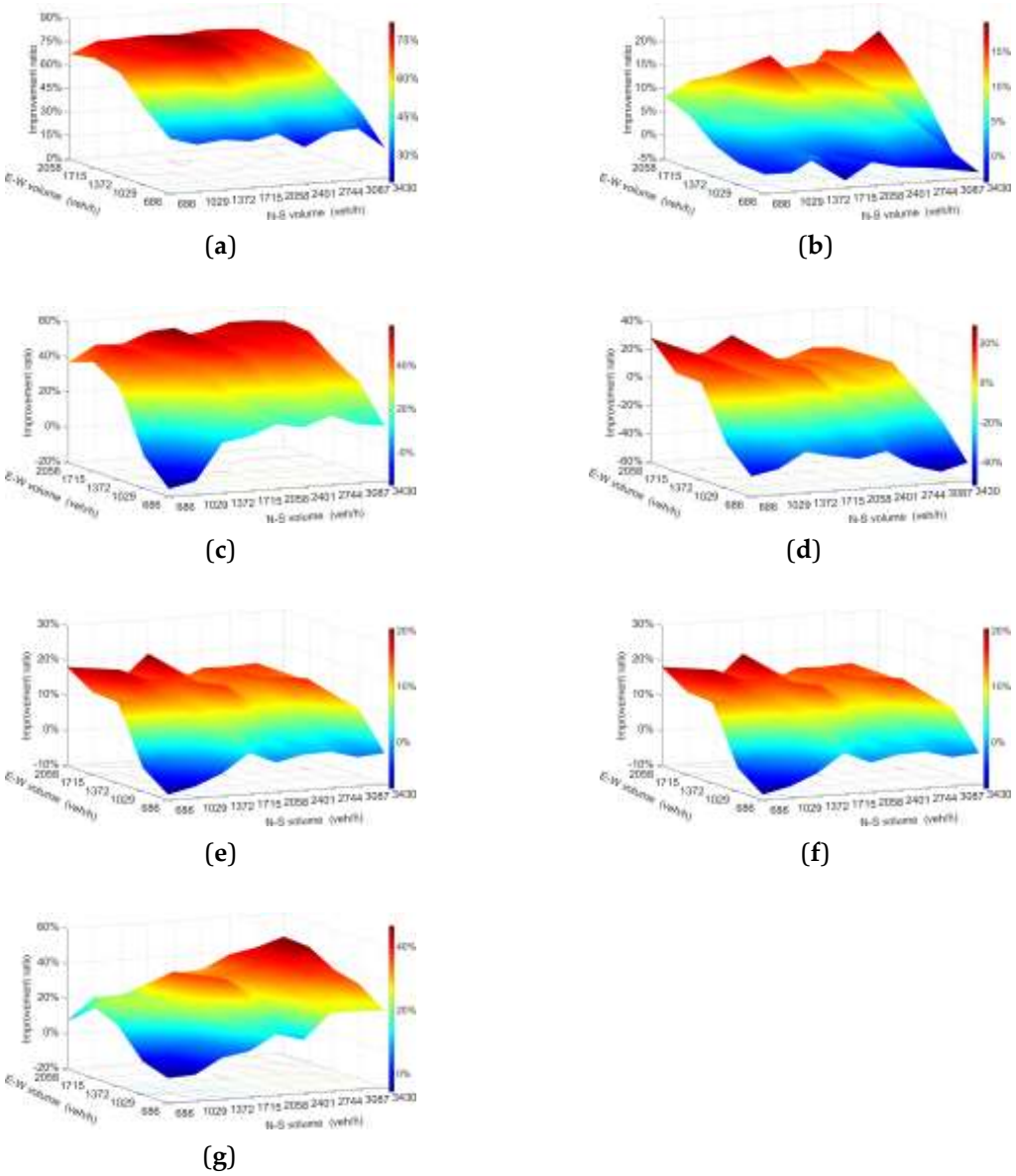

Figure 9. Improvement ratio of CFI, compared with conventional solution: (**a**) maximum queue length; (**b**) number of vehicles; (**c**) delay; (**d**) number of stops; (**e**) CO emissions; (**f**) fuel consumption; and (**g**) travel time.

Figure 9e,f represent the comparison of CO emissions and fuel consumption between the two solutions, respectively. In contrast to USC, the CO emissions and fuel consumption of CFI were more than those of the conventional solution only when the east–west and north–south traffic volumes were small, with a maximum of only 8.5%. As the traffic volume increased, especially in the east–west direction, the CFI improvement incrementally increased, reaching a maximum of 20.3%.

Figure 9g shows the degree of improvement of CFI for vehicle travel time. The improvement of CFI was not satisfactory, with a magnitude of −5.8% at low east–west and north–south traffic volumes, representing that CFI was not as good as the conventional solution at low traffic volumes. However, in the vast majority of cases, the improvement

ISSN: 2278-4632
Vol-12 Issue-07 No.03 July 2022

of CFI was better, with the same trend of optimization as the USC—gradually increasing as the traffic volume in the east–west and north–south directions increases from small to large—reaching a maximum of 46.4%.

Figure 10a reflects the degree of improvement of PFI for the maximum queue length. The overall trend in the degree of optimization was similar to that of USC, with PFI performing well in most cases. When the traffic volume in the east–west direction was very small and the traffic volume in the north–south direction was very high, the degree of improvement of PFI was poor, with the worst reaching –88.1%. When the north–south traffic volume was less than 2744 veh/h, the maximum queue lengths of PFI were all smaller than those of the conventional solution, and the degree of improvement gradually grew as the traffic volume in the east–west direction expanded, with the maximum reaching 86.0%.

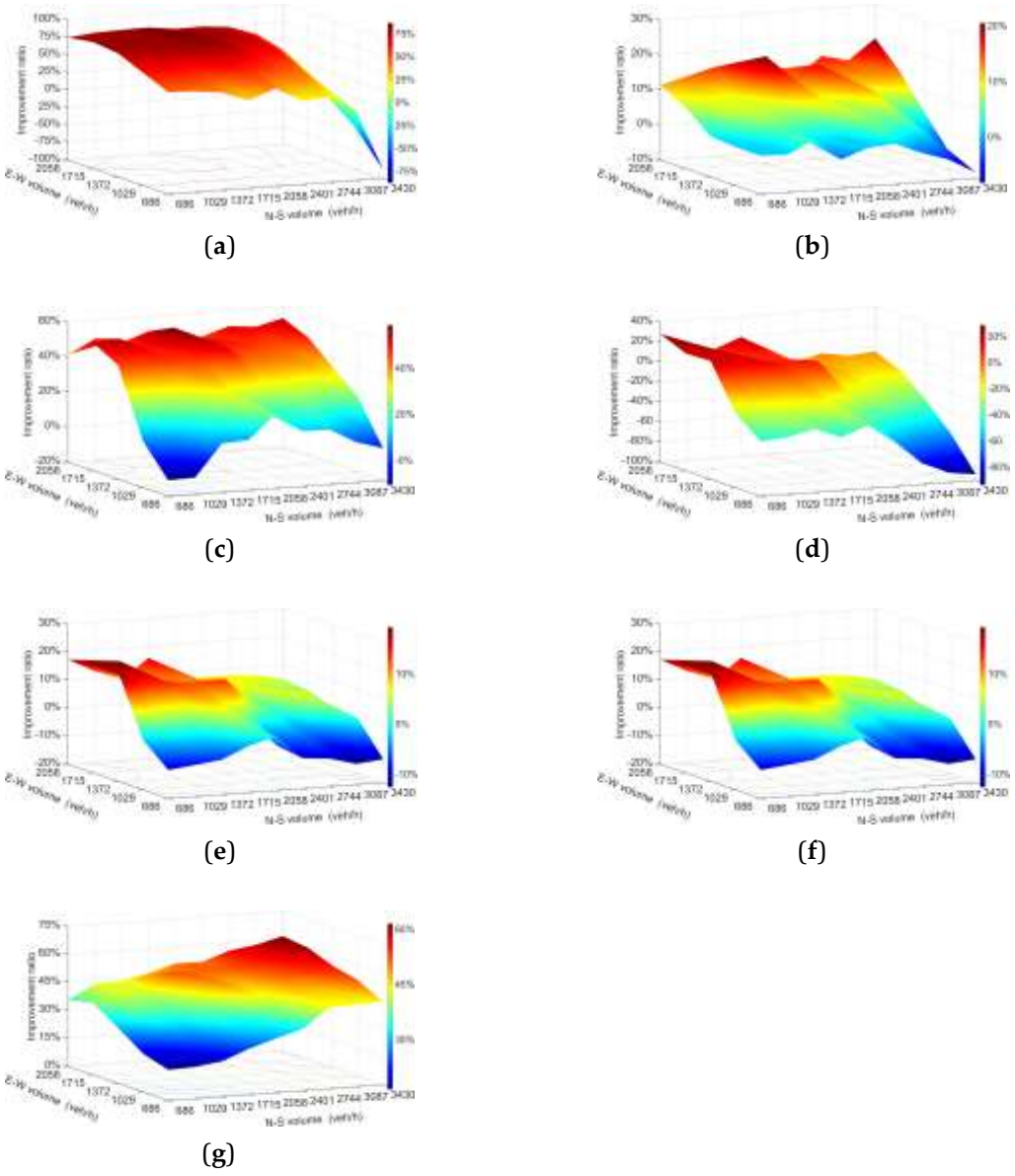

Figure 10. Improvement ratio of PFI, compared with conventional solution: (**a**) maximum queue length; (**b**) number of vehicles; (**c**) delay; (**d**) number of stops; (**e**) CO emissions; (**f**) fuel consumption; and (**g**) travel time.

ISSN: 2278-4632
Vol-12 Issue-07 No.03 July 2022

Figure 10b shows that the PFI had greater capacity than the conventional solution in most cases, with a favorable improvement and a similar trend to the CFI. When the traffic volume in the east–west direction was small and the traffic volume in the north–south direction was large, PFI was not as good as the conventional intersection, being 8.3% worse than the conventional scheme. As the traffic volume in the east–west and north–south directions increased, the degree of improvement gradually increased and reached a maximum of 20.4%.

Figure 10c reflects the results of PFI for the improvement of delays, with trends and regularities generally consistent with those of CFI. In the overwhelming majority of cases, PFI was better than the conventional solution. When both east–west and north–south traffic volumes were extremely low, the delays of the PFI were slightly higher than those of the conventional solution, reaching a maximum of 10.9%, but as the east–west and north–south traffic volumes gradually increased, the delays of the PFI were significantly reduced, compared to the conventional solution, with a maximum reduction of 58.5%.

Figure 10d shows the improvement of the PFI for the number of stops. From the figure, it is obvious that, in the overwhelming majority of cases, PFI had a greater number of stops than the conventional solution, by up to 52.1%. In some cases, PFI was similar to CFI. The PFI outperformed the conventional solution, with a maximum improvement of 28.8%, only when there was a high volume of east–west traffic and a low volume of north–south traffic.

Figure 10e,f reflect the improvement of PFI for CO emissions and fuel consumption, showing a similar regularity to CFI. When the traffic volume in the east–west direction was very small, PFI was worse than the conventional solution, by up to 8.5%. As the traffic volume in the east–west direction increased, the improvement in the PFI gradually increased, reaching a maximum of 20.3%.

Figure 10g indicates that, in all cases, the vehicle travel time of PFI was less than that of the conventional solution, providing significant improvement. Similar to CFI, the degree of improvement of PFI gradually increased when the traffic volume in the east–west and north–south directions increased, with the lowest improvement of 16.4% when the traffic volume in the east–west and north–south directions was small. The greatest improvement (61.3%) was achieved in the case of the highest traffic volumes in the east–west and north–south directions.

Figures 8–10 indicate that, overall, CFI and PFI improved upon the conventional solution more than USC. For the three indices of delay, travel time, and number of vehicles, the degree of improvement of the three unconventional intersections was significant, indicating that all three intersections could improve the operations of different traffic flows at the intersection, especially left-turning traffic flows, through unique traffic organization, effectively improving the capacity of the intersection and reducing delays. From the results, it can be seen that the number of stops for the three unconventional intersections was significantly higher than that for the conventional intersection, which was due to the existence of four additional secondary intersections in all three improvement solutions. Regarding CFI and PFI, it can be seen that the trends and regularities of the degree of improvement of these two intersections had relatively large similarities, and the minimum and maximum improvement are close to each other, such that it is worth considering which intersection has the best comprehensive performance, in terms of optimization, under any different combination of traffic volumes.

5. Analysis of the Results Based on the Critic Method

The CRITIC (CRiteria Importance Through Intercriteria Correlation) method is a better objective assignment method than the entropy method or the standard deviation method. Its basic philosophy is to determine the objective weights of the indices based on two fundamental concepts [64]: The first is the contrast intensity, which indicates the size of the gap between the values of each evaluation scheme for the same indicator, in the form of standard deviation; that is, the size of the standard deviation indicates the size of the discrepancy between the values of each scheme within the same indicator—

ISSN: 2278-4632
Vol-12 Issue-07 No.03 July 2022

the larger the standard deviation, the larger the gap between the values of each scheme. The second is the conflicting character of the evaluation criteria, based on the correlation between indices; for example, a strong positive correlation between indices indicates that the conflicting character between two indices is low. The CRITIC method provides a comprehensive measure of the objective weights of indices, based on the contrast intensity of the evaluation indices and the conflicting character between them. It takes into account the correlation between the indices while considering the magnitude of the variability of the indices, meaning that the results are not evaluated according only to the largeness of the number, but the objective properties of the data are fully used to ensure scientific and comprehensive evaluation. Therefore, for indices such as delays, travel time, number of stops, number of vehicles, CO emissions, and fuel consumption, it is appropriate to use the CRITIC method to analyze their weights in a comprehensive manner.

5.1. Calculation of Weighting of Indices

In the sensitivity analysis, simulations were performed for the four considered solutions under a total of 45 different combinations of traffic volumes. Seven indices were selected for the analysis. Hence, each solution had a set of simulation results for each group of traffic volumes.

Step 1. All simulation results under each solution are summarized as the matrix A_i (3):

$$A_i = [Qu_{i,k}, Ve_{i,k}, De_{i,k}, St_{i,k}, Co_{i,k}, Fu_{i,k}, Tr_{i,k}] \quad (3)$$

where i denotes the solution number ($i = 1, 2, 3, 4$, where the conventional solution, USC, CFI, and PFI are represented as 1, 2, 3 and 4, respectively), k denotes the number of traffic volume groups ($k = 1, 2, \cdots, 45$), Qu denotes the maximum queue length, Ve denotes the number of vehicles, De denotes delays, St denotes the number of stops, Co denotes CO emissions, Fu denotes fuel consumption, and Tr denotes travel time.

For example:

$$A_1 = [Qu_{1,k}, Ve_{1,k}, De_{1,k}, St_{1,k}, Co_{1,k}, Fu_{1,k}, Tr_{1,k}]$$

in the formula:

$$Qu_{1,k}=[Qu_{1,1}, Qu_{1,2}, Qu_{1,3}, \cdots, Qu_{1,45}]^T$$

The four matrices $A1$, $A2$, $A3$, and $A4$ represent the simulation results of each solution under all combinations of traffic volumes. To compare the differences in the indices between the different solutions, the simulation results of different solutions need to be recombined and then computed and analyzed.

Step 2. The simulation results of all solutions under the same combination of traffic volumes are summarized in the matrix X_k (4):

$$X_k = \begin{matrix} A_1(k, \cdot) \\ A_2(k, \cdot) \\ A_3(k, \cdot) \\ A_4(k, \cdot) \end{matrix} \quad (4)$$

and

$$X=[X_1, X_2, X_3 \cdots X_k \cdots X_{45}]^T \quad (5)$$

where $A_1(k,\cdot)$ denotes the kth row of A_1 (i.e., the simulation results obtained for the first solution under the kth group of traffic).

Step 3. The weights of the seven indices are calculated. For each component X_k in X, the weights are counted once, which means that there is a set of weights for each of the seven indices selected for the four different solutions under each combination of traffic volume, for a total of 45.

ISSN: 2278-4632
Vol-12 Issue-07 No.03 July 2022

$$X_k = \begin{matrix} Qu_{1,k}, Ve_{1,k}, De_{1,k}, St_{1,k}, Co_{1,k}, Fu_{1,k}, Tr_{1,k} \\ Qu_{2,k}, Ve_{2,k}, De_{2,k}, St_{2,k}, Co_{2,k}, Fu_{2,k}, Tr_{2,k} \\ Qu_{3,k}, Ve_{3,k}, De_{3,k}, St_{3,k}, Co_{3,k}, Fu_{3,k}, Tr_{3,k} \\ Qu_{4,k}, Ve_{4,k}, De_{4,k}, St_{4,k}, Co_{4,k}, Fu_{4,k}, Tr_{4,k} \end{matrix}$$

Under the kth combination of traffic volume, for X_k, a 4×7 matrix containing the weights of each index is calculated, based on the CRITIC method, as follows:

(1) Each element in matrix X_k is denoted by y_{ij}, where i denotes the ith solution, n denotes the total number of solutions (totaling 4), j denotes the jth index, and m denotes the total number of indices (totaling 7):

$$Y = y_1, y_2, \cdots y_j \cdots y_7 \tag{6}$$

in the formula:

$$y_j = y_{1j}, y_{2j}, y_{3j}, y_{4j}^T$$

The seven selected indices—maximum queue length, number of vehicles, delays, number of stops, CO emissions, fuel consumption, and travel time—are numbered 1 to 7, respectively. Of these indices, all are expected to be low; except for the number of vehicles, which is expected to be high. Therefore, the indices need to be normalized. The specific method is shown in (7):

$$y_j' = \begin{matrix} \max\{y_{1j}, y_{2j}, y_{3j}, y_{4j}\} - y_{1j} \\ \max\{y_{1j}, y_{2j}, y_{3j}, y_{4j}\} - y_{2j} \\ \max\{y_{1j}, y_{2j}, y_{3j}, y_{4j}\} - y_{3j} \\ \max\{y_{1j}, y_{2j}, y_{3j}, y_{4j}\} - y_{4j} \end{matrix}, j = 2. \tag{7}$$

The resulting Y' (8) is obtained as:

$$Y' = y_1', y_2', \cdots, y_j', \cdots, y_7' \tag{8}$$

where $y_2' = y_2$.

(2) The different indices have different scales and they need to be converted into a uniform scale for comparison. Thus, they need to be normalized (i.e., the absolute indices are converted into relative ones). Each element of Y', denoted by y_{ij}', is normalized using (9):

$$y_{ij}'' = \frac{y_{ij}' - \min(y_{1j}', \cdots, y_{4j}')}{\max(y_{1j}', \cdots, y_{4j}') - \min(y_{1j}', \cdots, y_{4j}')} \tag{9}$$

$$i = 1 \text{ to } n, j = 1 \text{ to } m.$$

The newly obtained combination of elements is $Y''_{4\times7}$.

(3) Calculate the variability of each solution at the jth index, expressed as the standard deviation, which is calculated by (10) and (11):

$$\overline{y''}_j = \frac{1}{n}\sum_{i=1}^{n} y''_{ij} \tag{10}$$

$$S_j = \sqrt{\frac{\sum_{i=1}^{n} (y''_{ij} - \overline{y''}_j)^2}{n-1}} \tag{11}$$

The standard deviation is used in the CRITIC method to indicate the difference and fluctuation of the values taken within each index. A larger standard deviation indicates a greater difference in the values of the index, more information that can be reflected, and a

ISSN: 2278-4632
Vol-12 Issue-07 No.03 July 2022

stronger evaluation intensity of the index itself, such that more weight should be assigned to the index.

(4) Calculate the conflicting character of the indices using (12):

$$R_j = \sum_{j'=1}^{m} 1 - r_{j,j'} \quad , j = 1 \text{ to } 7, \tag{12}$$

where R_j denotes the correlation index of the jth index and $r_{j,j'}$ denotes the correlation coefficient of the jth and j'th indices.

The correlation index is used to express the correlation between indices. The stronger the correlation with other indices, the less conflicting the index is, the more the same information is reflected, and the more duplication in the evaluation content that can be embodied; which, to some extent, also weakens the evaluation strength of the index and should reduce the weight assigned to the index.

(5) Calculate the amount of information using (13):

$$C_j = S_j \times R_j = S_j \cdot \sum_{j'=1}^{m} 1 - r_{j,j'} \quad , j = 1 \text{ to } 7. \tag{13}$$

A larger value of C_j indicates that the jth evaluation index plays a greater role in the whole evaluation index system, and it should be assigned more weight.

(6) Calculation of objective weights: For the ith solution, the objective weight of the jth index under the kth group of traffic combinations is calculated by (14):

$$w_{k,j} = \frac{C_j}{\sum_{j=1}^{m} C_j} \tag{14}$$

Under each set of traffic volume combinations, there is a set of weights:

$$W_k = \left[w_{k,1}, w_{k,2}, \cdots, w_{k,j}, \cdots, w_{k,7} \right]$$

The calculated values of all weights are attributed to (15):

$$W = [W_1, W_2, \cdots, W_k, \cdots, W_{45}]^T \tag{15}$$

5.2. Evaluation of Solutions

According to the weights of the different indices, each solution can be scored in a comprehensive manner, as follows:

For the case of the kth group of traffic combinations.

(1) In the simulation results of the jth index, the ratio of the value of the ith solution to the value of all solutions can be obtained using (16):

$$p_{ij} = \frac{y''_{ij}}{\sum_{i=1}^{n} y''_{ij}}, j = 1 \text{ to } 7. \tag{16}$$

(2) The score of the ith solution in index j can be calculated by (17):

$$z_{ij} = w_{ij} \times p_{ij}, i = 1 \text{ to } 4, j = 1 \text{ to } 7. \tag{17}$$

(3) Calculate the total score of the ith solution by (18):

$$z_i = \sum_{j=1}^{7} z_{ij}, i = 1 \text{ to } 4. \tag{18}$$

ISSN: 2278-4632
Vol-12 Issue-07 No.03 July 2022

(4) The total score of all solutions is expressed as a matrix Z_k (19):

$$Z_k = [z_1, z_2, z_3, z_4]^T \tag{19}$$

The scores for each solution under all combinations of traffic volumes are summarized in Z (20):

$$Z = [Z_1, Z_2, \cdots, Z_k, \cdots, Z_{45}]^T \tag{20}$$

Then, we can pick the best solution for each case by (21):

$$B = \begin{matrix} i, if\ z_i = \max Z_1 \\ i, if\ z_i = \max Z_2 \\ \vdots \\ i, if\ z_i = \max Z_{45} \end{matrix} \tag{21}$$

The optimal solution matrix, B, is represented in Figure 10. The 45 squares represent the group of 45 traffic volume cases, where each color block represents the comprehensive optimal solution.

From Figure 11, it can be seen that there was a certain regularity in the distribution of the whole color block picture. The conventional solution occupies the lower left part, indicating that the conventional solution was adapted to low traffic volume. The PFI occupies the middle part, indicating that the PFI is more suitable for moderate and high traffic volumes. The CFI occupies the upper right corner of the figure, indicating that the CFI is applicable to situations with high traffic volumes. USC does not appear in the figure as, although it provides the good improvement, compared to the conventional solution, at certain traffic volumes, it is dwarfed by CFI and PFI.

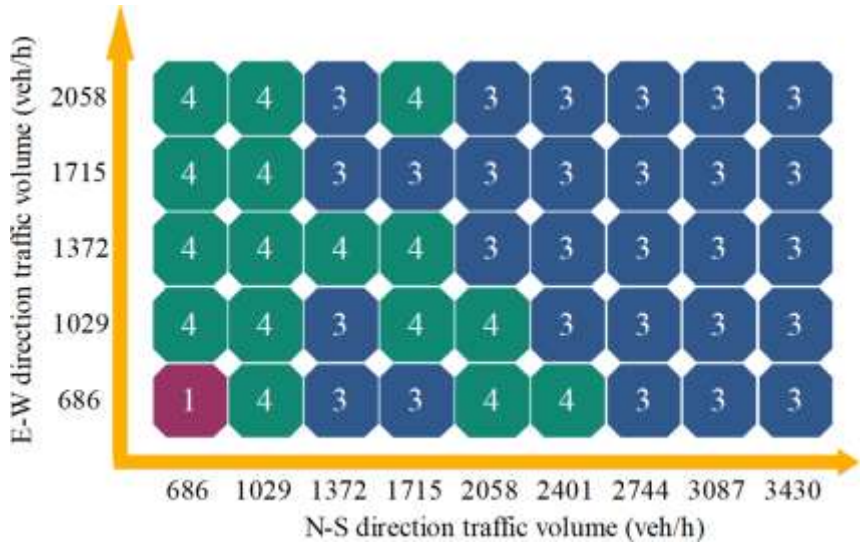

Figure 11. The optimal solution for each traffic situation. The numbers in the figure represent the solution number, and the number indicates the best performance among the four solutions for one volume combination.

Figure 11 shows the optimal solution obtained by the multi-criteria decision-making method, considering traffic and environmental indices, but this optimal solution only indicates the best comprehensive performance and does not necessarily perform well under each of the indices. The optimal comprehensive solution represented in Figure 11 is now used for comparison with the conventional solution. The results are shown in Figure 12.

Figure 12a,g show the results comparing the maximum queue length and travel time based on the improved solution and the conventional solution, respectively. It is

ISSN: 2278-4632
Vol-12 Issue-07 No.03 July 2022

clear that, for the two indices, the selected solution had a better overall improvement, with no negative improvement for both and with maximum improvements of 81.7% and 46.9%, respectively. When the traffic volume was 686 veh/h in the east–west direction and north–south direction, the improvement was the lowest.

Figure 12b shows the comparison of the number of vehicles. In the range of traffic volumes in the east–west direction less than 686 veh/h, the improvement was not very good: 3.8% worse than the conventional solution. The selected solution was better in the vast majority of cases, with the greatest improvement of 19.2% when the traffic volume reached its maximum.

Figure 12c indicates that the selected solution performed better, in terms of delays, in the vast majority of cases, with a maximum of 58%. It was inferior to the original solution only when both east–west and north–south traffic volumes were at a minimum of 686 veh/h, with an improvement of −10.5%.

Figure 12d shows the degree of improvement for the number of stops. Obviously, when the traffic volume in the east–west direction was less than 1372 veh/h, the improvement in the number of stops was poor—with negative improvement—which means that the improved solution was not as good as the conventional solution, with the worst being 56% worse than the conventional solution. The improvement of the selected solution was better only when the traffic volume was greater than 2058 veh/h in the east–west direction, with a maximum of 28.2%.

Figure 12e,f show the comparison between the improved solution and the conventional solution for the indices of CO emissions and fuel consumption, respectively. The trends are almost identical in both graphs. The conventional solution was better when the traffic volume was low, especially when the east–west traffic volume was less than 1029 veh/h, but the selected solution was only about 2% worse than the conventional solution.

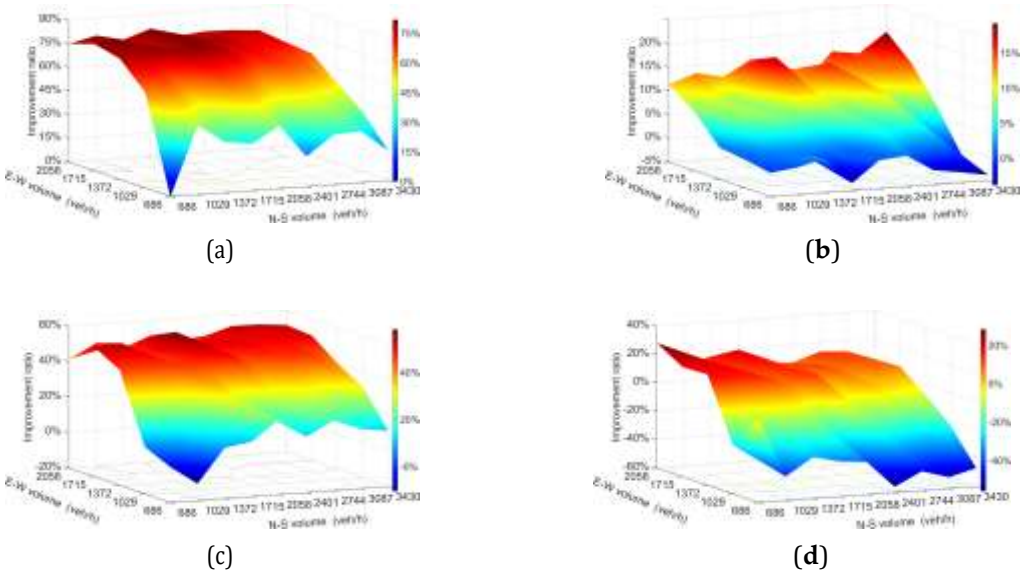

(a) (b)

(c) (d)

Figure 12. *Cont.*

ISSN: 2278-4632
Vol-12 Issue-07 No.03 July 2022

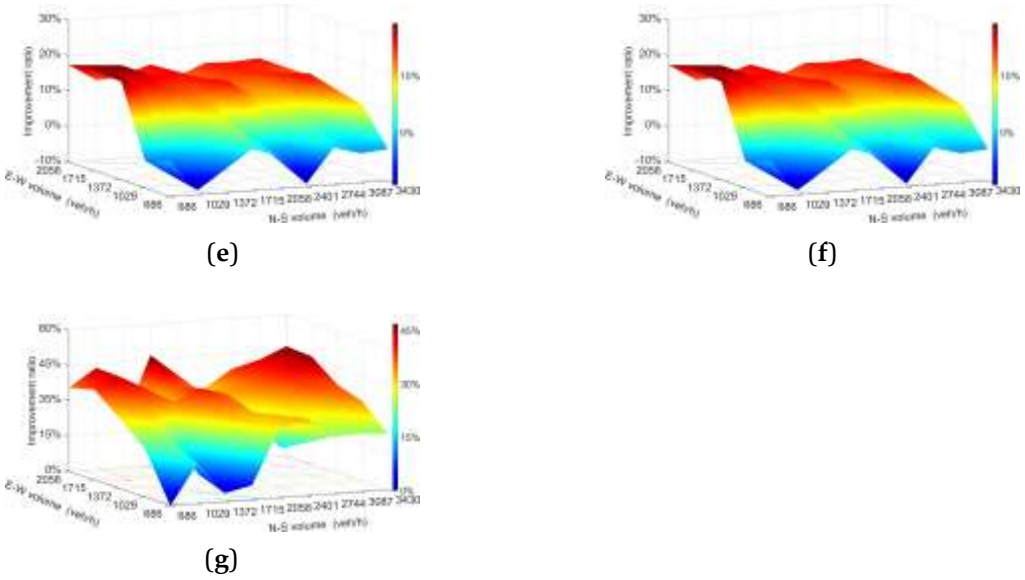

Figure 12. Operating performance of the matrix in Figure 11 matrix: (**a**) maximum queue length; (**b**) number of vehicles; (**c**) delay; (**d**) number of stops; (**e**) CO emissions; (**f**) fuel consumption; and (**g**) travel time.

6. Conclusions

The transportation networks in Chinese cities have been developing at an extremely fast pace. With the rapid growth of the urban population and the increase in the number of vehicles, urban roads are already overburdened, and the current main measures to deal with urban road congestion are banning non-local vehicles and restricting local vehicles, which not only cannot effectively solve the problem of urban road congestion [95], but also adversely affects citizens and regional economic development. For a rapidly developing city, if conventional intersections are still always used for the design and construction of new projects, the intersection will soon reach a bottleneck and not only fail to meet the requirements of the road network, but the cost of later modification and expansion will also not be cheap. As a result, many cities have gradually adopted unconventional intersections, in order to better utilize the potential of intersection junctions, improving their capacity while ensuring cost savings and better aesthetic appearance.

For USC, CFI, and PFI, three commonly used unconventional intersections, how to select to achieve better performance is a question worth researching. With the current society focusing increasingly on the concept of eco-friendly sustainability, it is important and imperative to consider not only the traffic performance of the solution, but also the environmental impact. In this paper, the maximum queue length, number of stops, number of vehicles, delays, and travel time were selected as traffic indices, while CO emissions and fuel consumption were selected as environmental indices for a conventional solution and three unconventional solutions. Then, a multi-criteria decision-making method based on CRITIC was used to carry out a comprehensive evaluation of the four solutions.

The results showed that the conventional solution can be used when the traffic volume is very low (i.e., less than 1029 veh/h in the east–west and north–south directions). PFI saves costs and performs better when the traffic volumes are moderate or high, such as when east–west and north–south traffic volume do not exceed 2058 veh/h. CFI is undoubtedly the best choice when the traffic volume is high in the east–west and north–south directions (i.e., over 2058 veh/h). The results of this paper do not conflict with those of previous studies, but are more comprehensive and refined.

This research mainly applied to the current intersection and it is appropriate for other similar intersections. In this paper, we obtained that USC, CFI, and PFI show different advantages and disadvantages in diverse situations. This regularity has a certain reference

ISSN: 2278-4632
Vol-12 Issue-07 No.03 July 2022

value because the sensitivity analysis on traffic volume is done for different solutions in this paper, which takes into account a more comprehensive traffic volume situation. In a rapidly developing city such as Xi'an, the design and construction of new intersections and the reconstruction of old intersections can be made more scientific by using unconventional intersection designs, which are of great significance in reducing delays, stopping times, and disturbances at intersections, as well as improving traffic capacity, saving energy, and protecting the environment. The CRITIC method used in this paper can serve as a guide for decision-makers, designers, or management, in terms of answering the question of which intersection should be selected under different traffic conditions.

Limitations of the research and the future steps: 1. This paper only considered structurally symmetrical four-legged unconventional intersections. In some cases, depending on the requirements, unconventional designs may be adopted for only one or two arms of the intersection. This asymmetric structure and layout may make it necessary to reevaluate the results. The authors will focus on these issues in future studies. 2. This paper only considers the vehicle types and proportion of left-turning vehicles collected at the current intersection. The increase in the number of left-turning vehicles and the proportion of large vehicles will have a significant impact on the traffic flow at intersections. Therefore, a more comprehensive consideration is needed in future studies. 3. The impact of building area of the three solutions is not considered, so the advantage of a small building area of PFI cannot be represented in the evaluation, which may have an impact on the final scoring results. Environmental indices such as building area will be considered in future studies and they could be converted into a generalized index, such as a monetary unit, which may be more conducive to evaluating the solutions.

References

1. Al-Dabbagh, M.S.M.; Al-Sherbaz, A.; Turner, S. The impact of road intersection topology on traffic congestion in urban cities. In *Intelligent Systems and Applications, IntelliSys 2018, Advances in Intelligent Systems and Computing*; Arai, K., Kapoor, S., Bhatia, R., Eds.; Springer: Cham, Switzerland, 2018; Volume 868.
2. Stevanovic, A.; Mitrovic, N.; Traffic microsimulation for flexible utilization of urban roadways. *Transp. Res. Rec. J. Transp. Res. Board* **2019**, *2673*, 92–104. [CrossRef]
3. Wang, H.; Luo, S.; Luo, T. Fractal characteristics of urban surface transit and road networks: Case study of Strasbourg, France. *Adv. Mech. Eng.* **2017**, *9*. [CrossRef]
4. Ma, M.; Yang, Q.; Liang, S.; Wang, Y. A new coordinated control method on the intersection of traffic region. *Discret. Dyn. Nat. Soc. Hindawi* **2016**, *2016*, 1–10. [CrossRef]
5. Li, S.; Li, G.; Cheng, Y.; Ran, B. Intersection congestion analysis based on cellular activity data. *IEEE Access* **2020**, *8*, 43476–43481. [CrossRef]
6. Chen, K.; Zhao, J.; Knoop, V.L.; Gao, X. Robust signal control of exit lanes for left-turn intersections with the consideration of traffic fluctuation. *IEEE Access* **2020**, *8*, 42071–42081. [CrossRef]
7. Sun, X.; Lin, K.; Jiao, P.; Lu, H. The dynamical decision model of intersection congestion based on risk identification. *Sustainability* **2020**, *12*, 5923. [CrossRef]
8. Astarita, V.; Caliendo, C.; Giofre`, V.P.; Russo, I. Surrogate safety measures from traffic simulation: Validation of safety indicators with intersection traffic crash data. *Sustainability* **2020**, *12*, 6974. [CrossRef]
9. Chen, J.; Wang, W.; Li, Z. Dispersion effect in left-turning bicycle traffic and its influence on capacity of left-turning vehicles at signalized intersections. *Transp. Res. Rec. J. Transp. Res. Board* **2014**, *2468*, 38–46. [CrossRef]
10. Zhang, H.; Jiang, R.; Hu, M.; Jia, B. Analytical investigation on the minimum traffic delay at a three-phase signalized t-type intersection. *Mod. Phys. Lett. B* **2017**, *31*, 1–9. [CrossRef]

11. Yan, Y.; Qu, X.; Li, H. On the design and operational performance of waiting areas in at-grade signalized intersections: An overview. *Transp. A Transp. Sci.* **2018**, *14*, 901–928. [CrossRef]
12. Yang, Q.; Shi, Z. Effects of the design of waiting areas on the dynamic behavior of queues at signalized intersections. *Phys. A Stat. Mech. Appl.* **2018**, *509*, 181–195. [CrossRef]
13. Hao, W.; Ma, C.; Moghimi, B.; Fan, Y.; Gao, Z. Robust optimization of signal control parameters for unsaturated intersection based on tabu search-artificial bee colony algorithm. *IEEE Access* **2018**, *6*, 32015–32022. [CrossRef]
14. Hao, W.; Lin, Y.; Cheng, Y.; Yang, X. Signal progression model for long arterial: Intersection grouping and coordination. *IEEE Access* **2018**, *6*, 30128–30136. [CrossRef]
15. Li, J.; Wang, W.; Zuylen, H.J.; Sze, N.N.; Chen, X.; Wang, H. Predictive Strategy for Transit Signal Priority at Fixed-Time Signalized Intersections: Case Study in Nanjing, China. *Transp. Res. Record* **2012**, *2311*, 124–131. [CrossRef]
16. Cruz-Piris, L.; Lopez-Carmona, M.A.; Marsa-Maestre, I. Automated optimization of intersections using a genetic algorithm. *IEEE Access* **2019**, *7*, 15452–15468. [CrossRef]
17. Małecki, K. The Importance of Automatic Traffic Lights time Algorithms to Reduce the Negative Impact of Transport on the Urban Environment. *Transp. Res. Procedia* **2016**, *16*, 329–342.
18. Jia, H.; Lin, Y.; Luo, Q.; Li, Y.; Miao, H. Multi-objective optimization of urban road intersection signal timing based on particle swarm optimization algorithm. *Adv. Mech. Eng.* **2019**, *11*. [CrossRef]
19. Małecki, K.; Pietruszka, P. Comparative Analysis of Chosen Adaptive Traffic Control Algorithms. *Recent Adv. Traffic Eng. Transp. Netw. Syst.* **2017**, *21*, 193–202.
20. Hu, W.; Wang, H.; Du, B.; Yan, L. A multi-intersection model and signal timing plan algorithm for urban traffic signal control. *Transport* **2014**, *32*, 368–378. [CrossRef]
21. Kim, D.; Jeong, O. Cooperative traffic signal control with traffic flow prediction in multi-intersection. *Sensors* **2020**, *20*, 37. [CrossRef]
22. Ren, C.; Wang, J.; Qin, L.; Li, S.; Cheng, Y. A novel left-turn signalcontrol method for improving intersection capacity in a connected vehicle environment. *Electronics* **2019**, *8*, 1058. [CrossRef]
23. Shu, S.; Zhao, J.; Han, Y. Signal timing optimization for transit priority at near-saturated intersections. *J. Adv. Transp.* **2018**, *2018*, 1–14. [CrossRef]
24. Dai, G.; Wang, H.; Wang, W. A bandwidth approach to arterial signal optimisation with bus priority. *Transp. A Transp. Sci.* **2015**, *11*, 579–602. [CrossRef]
25. Dai, G.; Wang, H.; Wang, W. Signal Optimization and Coordination for Bus Progression Based on MAXBAND. *KSCE J. Civ. Eng.* **2016**, *20*, 890–898. [CrossRef]
26. Zhao, J.; Liu, Y.; Yang, X. Operation of signalized diamond interchanges with frontage roads using dynamic reversible lane control. *Transp. Res. Part C Emerg. Technol.* **2015**, *51*, 196–209. [CrossRef]
27. Zhao, J.; Ma, W.; Zhang, H.M.; Yang, X. Increasing the capacity of signalized intersections with dynamic use of exit lanes for left-turn traffic. *Transp. Res. Rec. J. Transp. Res. Board* **2013**, *1*, 49–59. [CrossRef]
28. Wu, J.; Liu, P.; Tian, Z.Z.; Xu, C. Operational analysis of the contraflow left-turn lane design at signalized intersections in china. *Transp. Res. Part C Emerg. Technol.* **2016**, *69*, 228–241. [CrossRef]
29. Shen, H.; Liu, D.; Liu, Z. The Same Entrance Full-Pass (SEFP) control method for the prevention of over-saturation at the critical intersection. *IEEE Access* **2020**, *8*, 143975–143984. [CrossRef]
30. Lee, J.; Park, B. Development and evaluation of a cooperative vehicle intersection control algorithm under the connected vehicles environment. *IEEE Trans. Intell. Transp. Syst.* **2012**, *13*, 81–90. [CrossRef]
31. Olsson, J.; Levin, M.W. Integration of microsimulation and optimized autonomous intersection management. *J. Transp. Eng. Part A Syst.* **2020**, *146*, 1–13. [CrossRef]
32. Miculescu, D.; Karaman, S. Polling-systems-based autonomous vehicle coordination in traffic intersections with no traffic signals. *IEEE Trans. Autom. Control* **2020**, *65*, 680–694. [CrossRef]
33. Esawey, M.; Sayed, T. Analysis of unconventional arterial intersection designs (UAIDs): State-of-the-art methodologies and future research directions. *Transp. A Transp. Sci.* **2013**, *9*, 860–895. [CrossRef]
34. Reid, J.D.; Hummer, J.E. Travel time comparisons between seven unconventional arterial intersection designs. *Transp. Res. Rec. J. Transp. Res. Board* **2001**, *1751*, 56–66. [CrossRef]
35. Naghawi, H.; AlSoud, A.; AlHadidi, T. The possibility for implementing the superstreet unconventional intersection design in Jordan. *Period. Polytech. Transp. Eng.* **2018**, *46*, 122–128. [CrossRef]
36. Tesoriere, G.; Campisi, T.; Canale, A.; Zgrablić, T. The surrogate safety appraisal of the unconventional elliptical and turbo roundabouts. *J. Adv. Transp.* **2018**, *2018*. [CrossRef]
37. Tollazzi, T.; Tesoriere, G.; Guerrieri, M.; Campisi, T. Environmental, functional and economic criteria for comparing "target roundabouts" with one-or two-level roundabout intersections. *Transp. Res. Part D Transp. Environ.* **2015**, *34*, 330–344. [CrossRef]
38. Coates, A.; Yi, P.; Koganti, S.; Du, Y. Maximizing intersection capacity through unconventional geometric design of two-phase intersections. *Transp. Res. Rec. J. Transp. Res. Board* **2012**, *2309*, 30–38. [CrossRef]
39. Shi, Z.; Luo, Q.; Zhang, S. Delay estimation and application conditions of two-legged continuous flow intersection. In Proceedings of the 2019 4th International Conference on Electromechanical Control Technology and Transportation (ICECTT), Guilin, China, 26–28 April 2019; pp. 53–56.

40. Yang, X.; Cheng, Y. Development of signal optimization models for asymmetric two-leg continuous flow intersections. *Transp. Res. Part C Emerg. Technol.* **2017**, *74*, 306–326. [CrossRef]
41. Esawey, M.; Sayed, T. Unconventional USC intersection corridors: Evaluation of potential implementation in Doha, Qatar. *J. Adv. Transp.* **2011**, *45*, 38–53. [CrossRef]
42. Sayed, T.; Storer, P.; Wong, G. Upstream Signalized Crossover intersection: Optimization and performance issues. *Transp. Res. Rec. J. Transp. Res. Board* **2006**, *1961*, 44–54. [CrossRef]
43. Gao, X.; Zhao, J.; Wang, M. Modelling the saturation flow rate for continuous flow intersections based on field collected data. *PLoS ONE* **2020**, *15*, e0236922.
44. You, X.; Li, L.; Ma, W. Coordinated optimization model for signal timings of full continuous flow intersections. *Transp. Res. Rec. J. Transp. Res. Board* **2013**, *2356*, 23–33. [CrossRef]
45. Yang, X.; Cheng, Y.; Chang, G. Operational analysis and signal design for asymmetric two-leg continuous-flow intersection. *Transp. Res. Rec. J. Transp. Res. Board* **2016**, *2553*, 72–81. [CrossRef]
46. Zhao, J.; Liu, Y.; Di, D. Optimization model for layout and signal design of full continuous flow intersections. *Transp. Lett.* **2016**, *8*, 194–204. [CrossRef]
47. Jagannathan, R.; Bared, J.G. Design and performance analysis of pedestrian crossing facilities for continuous flow intersections. *Transp. Res. Rec. J. Transp. Res. Board* **2005**, *1939*, 133–144. [CrossRef]
48. Sun, W.; Wu, X.; Wang, Y.; Yu, G. A continuous-flow-intersection-lite design and traffic control for oversaturated bottleneck intersections. *Transp. Res. Part C Emerg. Technol.* **2015**, *56*, 18–33. [CrossRef]
49. Kozey, P.; Xuan, Y.; Cassidy, M.J. A low-cost alternative for higher capacities at four-way signalized intersections. *Transp. Res. Part C Emerg. Technol.* **2016**, *72*, 157–167. [CrossRef]
50. Naghawi, H.H.; Idewu, W.I.A. Analysing delay and queue length using microscopic simulation for the unconventional intersection design Superstreet. *J. S. Afr. Inst. Civ. Eng.* **2014**, *56*, 100–107.
51. Shams, A.; Zlatkovic, M. Effects of capacity and transit improvements on traffic and transit operations. *Transp. Plan. Technol.* **2020**, *43*, 602–619. [CrossRef]
52. Gyawali, S.; Sharma, A.; Khattak, A.J.; Smaglik, E. Use of decision assistance curves in advanced warrant analysis for indirect left-turn intersections. *Transp. Res. Rec. J. Transp. Res. Board* **2015**, *2486*, 54–63. [CrossRef]
53. Jagannathan, R.; Bared, J.G. Design and operational performance of crossover displaced left-turn intersections. *Transp. Res. Rec. J. Transp. Res. Board* **2004**, *1881*, 1–10. [CrossRef]
54. Parsons, G.F. The parallel flow intersection: A new high capacity urban intersection. In Proceedings of the 5th Advanced Forum on Transportation of China (AFTC 2009), Beijing, China, 17 October 2009; pp. 143–150.
55. Dhatrak, A.; Edara, P.; Bared, J.G. Performance analysis of parallel flow intersection and displaced left-Turn intersection designs. *Transp. Res. Rec. J. Transp. Res. Board* **2010**, *2171*, 33–43. [CrossRef]
56. Esawey, M.E.; Sayed, T. Comparison of two unconventional intersection schemes: Crossover displaced left-turn and upstream signalized crossover intersections. *Transp. Res. Rec. J. Transp. Res. Board* **2007**, *2023*, 10–19. [CrossRef]
57. Cheong, S.; Rahwanji, S.; Chang, G. Comparison of three unconventional arterial intersection designs: Continuous Flow Intersection, Parallel Flow Intersection, and Upstream Signalized Crossover. In Proceedings of the 11th International IEEE Conference on Intelligent Transportation Systems, Beijing, China, 6 June 2008.
58. Autey, J.; Sayed, T.; Esawey, M.E. Operational performance comparison of four unconventional intersection designs using micro-simulation. *J. Adv. Transp.* **2013**, *47*, 536–552. [CrossRef]
59. Sahin, M. A comprehensive analysis of weighting and multicriteria methods in the context of sustainable energy. *Int. J. Environ. Sci. Technol.* **2020**. [CrossRef]
60. Kumar, A.; Sah,B.; Singh, A.R.; Deng, Y.; He, X.; Kumar, P.; Bansald, R.C. A review of multi criteria decision-making (MCDM) towards sustainable renewable energy development. *Renew. Sustain. Energy Rev.* **2017**, *69*, 596–609. [CrossRef]
61. Wu, Y.; Xu, C.; Zhang, T. Evaluation of renewable power sources using a fuzzy MCDM based on cumulative prospect theory: A case in China. *Energy* **2018**, *147*, 1227–1239. [CrossRef]
62. Shao, Y.; Han, X.; Wu, H.; Claudel, C.G. Evaluating signalization and channelization selections at intersections based on an entropy method. *Entropy* **2019**, *21*, 808. [CrossRef]
63. Shao, Y.; Luo, Z.; Wu, H.; Han, X.; Pan, B.; Liu, S.; Claudel, C.G. Evaluation of two improved schemes at non-aligned intersections affected by a work zone with an entropy method. *Sustainability* **2020**, *12*, 5494. [CrossRef]
64. Diakoulaki, D.; Mavrotas, D.G.; Papayannakis, L. Determining objective weights in multiple criteria problems: The critic method. *Comput. Oper. Res.* **1995**, *22*, 763–770. [CrossRef]
65. Kumari, M.; Kulkarni, M.S. A unified index for proactive shop floor control. *Int. J. Adv. Manuf. Technol.* **2019**, *100*, 2435–2454. [CrossRef]
66. Li, L.; Mo, R. Production task queue optimization based on multi-attribute evaluation for complex product assembly workshop. *PLoS ONE* **2017**, *10*, e0134343. [CrossRef]
67. Zhao, M.; Wang, X.; Yu, J.; Xue, L.; Yang, S. A construction schedule robustness measure based on improved prospect theory and the Copula-CRITIC method. *Appl. Sci.* **2020**, *10*, 2013. [CrossRef]
68. Ghorabaee, M.K.; Amiri, M.; Zavadskas, E.K.; Antucheviciene, J. A new hybrid fuzzy MCDM approach for evaluation of construction equipment with sustainability considerations. *Arch. Civ. Mech. Eng.* **2018**, *18*, 32–49. [CrossRef]

69. Obulaporam, G.; Somu, N.; Ramani, G.R.M.; Boopathy, A.K.; Sankaran, S.S.V. GCRITICPA: A CRITIC and grey relational analysis based service ranking approach for cloud service selection. In *Communications in Computer and Information Science*; Springer: Singapore, 2018; Volume 941.
70. Zhao, Q.; Zhou, X.; Xie, R.; Li, Z. Comparison of three weighing methods for evaluation of the HPLC fingerprints of Cortex Fraxini. *J. Liq. Chromatogr. Relat. Technol.* **2011**, *34*, 2008–2019. [CrossRef]
71. Lin, Z.; Wen, F.; Wang, H.; Lin, G.; Mo, T.; Ye, X. CRITIC-Based node importance evaluation in Skeleton-Network reconfiguration of power grids. *IEEE Trans. Circuits Syst. II Express Briefs* **2018**, *65*, 206–210. [CrossRef]
72. Marković, V.; Stajić, L.; Stević, Ž.; Mitrović, G.; Novarlić, B.; Radojičić, Z. A novel integrated Subjective-Objective MCDM model for alternative ranking in order to achieve business excellence and sustainability. *Symmetry* **2020**, *12*, 164.
73. San Cristo´bal, J.R. Multi-criteria decision-making in the selection of a renewable energy project in spain: The Vikor method. *Renew. Energy* **2011**, *36*, 498–502.
74. Lamas, M.I.; Castro-Santos, L.C.; Rodriguez, G. Optimization of a multiple injection system in a marine diesel engine through a Multiple-Criteria Decision-Making approach. *Mar. Sci. Eng.* **2020**, *8*, 946. [CrossRef]
75. Xi'an Government Homepage. Profile of Xi'an. 2020. Available online: http://en.xa.gov.cn/thisisxian/profile/944.htm (accessed on 23 October 2020).
76. Xi'an Municipal Bureau of Statistics. *2020 Xi'an Statistical Yearbook*; China Statistics Press: Beijing, China. Available online: http://tjj.xa.gov.cn/tjnj/2020/zk/indexeh.htm (accessed on 10 January 2021).
77. AutoNavi Traffic Big-Data. 2020. *Traffic Analysis Reports for Major Cities in China. 2020.Q3.* Available online: https://report.amap.com/share.do?id=a187b9ae753f219a01755470efdc6127 (accessed on 23 October 2020).
78. The Ministry of Public Security of the People's Republic. Available online: https://www.mps.gov.cn/n2254314/n6409334/index.html (accessed on 23 March 2021)
79. Coates, A.; Yi, P.; Liu, P.; Ma, X. Geometric and operational improvements at continuous flow intersections to enhance pedestrian safety. *Transp. Res. Rec. J. Transp. Res. Board* **2014**, *2436*, 60–69. [CrossRef]
80. Carroll, D.H.; Lahusen, D. Operational effects of continuous flow intersection geometrics: A deterministic model. *Transp. Res. Rec. J. Transp. Res. Board* **2013**, *2348*, 1–11. [CrossRef]
81. Yang, Z.; Liu, P.; Chen, Y.; Yu, H. Can left-turn waiting areas improve the capacity of left-turn lanes at signalized intersections? *Procedia Soc. Behav. Sci.* **2012**, *43*, 192–200. [CrossRef]
82. Milam, R.T.; Choa, F. Recommended guidelines for the calibration and validation of traffic simulation models. In Proceedings of the 8th TRB Conference on the Application of Transportation Planning Methods, Corpus Christi, TX, USA, 22–26 April 2002; pp. 178–187.
83. Park, B.; Won, J.; Yun, I. Application of microscopic simulation model calibration and validation procedure: Case study of coordinated actuated signal system. *Transp. Res. Rec. J. Transp. Res. Board* **2006**, *1978*, 113–122. [CrossRef]
84. Chu, L.; Liu, H.X.; Oh, J.S.; Recker, W. A calibration procedure for microscopic traffic simulation. In Proceedings of the 2003 IEEE International Conference on Intelligent Transportation Systems, Shanghai, China, 12–15 October 2003; Volume 2, pp. 1574–1579.
85. Sun, J. *Guideline for Microscopic Traffic Simulation Analysis*; Tongji University Press: Shanghai, China, 2014.
86. Xiang, Y.; Li, Z.; Wang, W.; Chen, J.; Wang, H.; Li, Y. Evaluating the operational features of an unconventional Dual-Bay U-Turn design for Intersections. *PLoS ONE* **2016**, *11*, e0163758. [CrossRef]
87. PTV AG. *PTV VISSSIM 10 User Manual*; PTV AG: Karlsruhe, Germany, 2018.
88. Henclewood, D.; Suh, W.; Rodgers, M.O.; Fujimoto, R.; Hunter, M.P. A calibration procedure for increasing the accuracy of microscopic traffic simulation models. *Simulation* **2017**, *93*, 35–47. [CrossRef]
89. Wang, J.; Mao, Y.; Li, J.; Xiong, Z.; Wang, W. Predictability of road traffic and congestion in urban areas. *PLoS ONE* **2015**, *10*, e0121825. [CrossRef] [PubMed]
90. Li, X.; Yang, T.; Liu, J.; Qin, X.; Yu, S. Effects of vehicle gap changes on fuel economy and emission performance of the traffic flow in the ACC strategy. *PLoS ONE* **2018**, *13*, e0200110. [CrossRef] [PubMed]
91. Federal Highway Administration Research and Technology. Surrogate Safety Assessment Model (SSAM). 2017. Available online: https://www.fhwa.dot.gov/publications/lists/020.cfm (accessed on 10 May 2020).
92. Federal Highway Administration (FHWA). *TECHBRIEF Surrogate Safety Assessment Model (SSAM)*; Federal Highway Administration: Washiton, DC, USA, 2008.
93. Federal Highway Administration (FHWA). *Surrogate Safety Assessment Model (SSAM)-SOFTWARE USER MANUAL*; Federal Highway Administration: Washiton, DC, USA, 2008.
94. Transportation Research Board (TRB). *Highway Capacity Manual, Sixth Edition: A Guide for Multimodal Mobility Analysis*; Transportation Research Board: Washiton, DC, USA, 2016.
95. Zhang, L.; Long, R.; Chen, H. Do car restriction policies effectively promote the development of public transport? *World Dev.* **2019**, *119*, 100–110. [CrossRef]